Predicting the size of stick-slip events: an in-depth look into the dynamics of a spring slider system

Msc Thesis G. van der Stelt, 307278, Utrecht University

31 May 2015

Abstract

Spring slider experiments are performed with a varying normal load, spring stiffness, load point velocity and grain size to determine the influence of these parameters on the displacement, force drop, maximum velocity and the reoccurrence time of a slip event and to validate the numerical model QDYN (Quasi DYNamic earthquake cycle simulator). The friction volume used, consist of spherical glass beads with a uniform grain size to create reproducible slip events (i.e. events with similar stress drops and displacements). The experimental results are used to validate QDYN, a numerical model based on rate-and-state friction laws. The rate-and-state friction parameters used by QDYN are fitted to the experimental data and the effect of changing these parameters on the displacement, force drop and maximum velocity is investigated. Using spherical glass beads as a friction volume the following trends where observed: An increase in the normal load results in a linear increase of the displacement, force drop and maximum velocity; An increase of the spring stiffness results in a negative power law relation with the measured variables and an increase of the load point velocity results in the increase of the measured variables according to a negative logarithmic law. It is shown that D_c cannot be used as a substitute for the grain size in QDYN. The spherical glass beads were substituted with angular quartz sand to determine what the effect of a different material is on rate-and-state parameters. The results show similar trends with the glass beads experiment. To obtain these results the RSF parameters used for the glass beads had to be adjusted: (a-b) increased, D_c decreased. We observed dependencies of dx, dF and Vmax on (a-b) and D_c using QDYN. Due to the quasi-dynamic nature of QDYN, the model is not capable of a precise prediction of the maximum size of an earthquake event, but can provide an approximation. The results of this study show similar relations to events found in nature and it is perhaps possible to extract RSF parameters of these events using large-scale simulation models such as QDYN.

1. Introduction

An earthquake is a natural phenomenon that is caused by sudden accelerating slip on a fault. During this slip energy is released in the form of seismic waves, heat production, frictional energy and fracture surface energy (Niemeijer et al., 2012). The seismic waves travel through the earth and cause shaking on the earth's surface, which can result in damage to buildings and loss of life. Since an earthquake is a recurring event predicting the maximum possible magnitude and slip of an earthquake can save lives, mitigate damage and help formulate building codes as well as insurance conditions. Most of the earthquakes are a consequence of lithospheric plate movement. This movement is translated into a build-up of stress in the subsurface which can lead to the formation of a fault or reactivation of an existing fault. In both cases, the fault is usually activated when stress exceeds the friction on the fault plane resulting in a sudden displacement along the fault. Because a fault is weaker than the surrounding rock, it is often a conductor through which stress is relieved, resulting in frequent reactivation of the fault. The consecutive reactivation of a fault is known as the seismic cycle (fig. 1). This unpredictable alternation between long periods of non-motion and sudden slip events is governed by a number of parameters such as stress conditions, loading velocity and frictional and elastic properties of the material involved.

The first aim of this study is to determine how the size of an earthquake is affected by these parameters. Experimental studies have been the backbone of research focused on the mechanisms of earthquakes, but an increasingly important role is reserved for studies based on numerical modelling. Numerical models can be used to simulate earthquake behaviour over a larger time-scale

than that available in either laboratory experiments (days, weeks, months) or that which spans the range of seismological data-sets (~100 years). One example of such a model is QDYN, a Quasi-DYNamic earthquake simulator that is capable of simulating a number of scenarios ranging from a simple spring slider analog to a complex 3D earthquake simulation. It is based on rate-and-state friction (RSF) laws, which describe the velocity dependence of friction (Dieterich, 1979; Ruina, 1983). QDYN is never used in comparison with laboratory experiments.

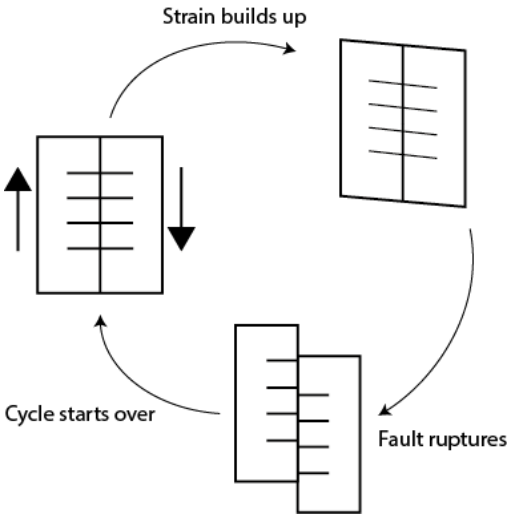

Figure 1 Schematic representation of the seismic cycle

The second aim of this study is to validate the results produced by the spring slider analog of QDYN to determine whether the model gives an accurate representation of the experimental data produced by a single degree of freedom spring (fig. 2). Since QDYN produces consistent results (i.e. events with constant amounts of slip, constant stress drops and constant peak slip velocities) when using constant RSF-values that do not mimic the heterogeneity of rocks found in nature, the experimental data has to be consistent as well, which we try to achieve by using uniformly sized spherical glass beads as the friction volume between the slider block and the underlying surface. Additional experiments have been performed using sub-angular quartz sand retrieved from an Ottawa sandstone to be able to make a comparison with materials occurring in the subsurface and to determine the effect of different RSF properties on the possible size of an earthquake. The experimental data acquired consists of the displacement, velocity, recurrence time and magnitude (force drop during the event) of multiple slip events while varying the normal load, spring stiffness, load point velocity and the grain size. The experimental results are compared with the results produced by QDYN with constant RSF parameters fitted to reproduce one particular event. Additionally, we investigated the effect of the RSF parameters on the displacement, force drop and maximum velocity using QDYN.

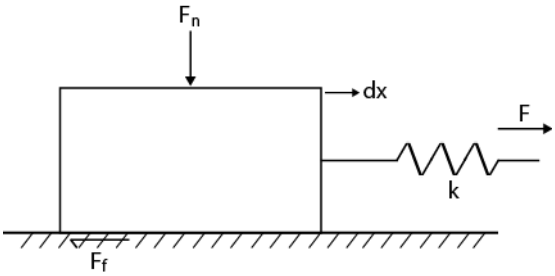

Figure 2 Schematic representation of a single degree spring slider system. The slider block is subjected to a constant normal force F_n, shear force F, friction force F_f and stress originating from the spring stiffness k. The slider block slips with displacement dx.

2. Theoretical background

Friction is the resistance a body undergoes when put in motion and has a contact surface with another body, i.e. the force that is needed to keep the body moving. The first concepts of friction and the laws it abides were tested and introduced by Leonardo da Vinci in the fifteenth century. He discovered the two main laws of friction, drew a distinction between sliding and rolling friction and observed that friction is less for smoother surfaces. He never published his findings, but they were rediscovered by Guillaume Amontons and published in 1699. He described the two main friction laws (Amontons, 1966):

- Amontons's first law: The frictional force is independent of the size of the surfaces in contact.
- Amontons's second law: Friction is proportional to the normal load.

In the years after the discovery of Amontons the importance of surface roughness was recognized, which was based on the concept of asperities (fig. 3), protrusions on the surface that interact and cause friction (Scholz, 2002). Two types of asperity interactions where proposed to explain how the interaction of asperities results in friction. The first type of interaction describes asperities acting as rigid springs creating friction because of the gravitational work done by asperities riding up and over one another. The second type of interaction describes asperities as elastic springs that deflect during sliding and cause friction. The concept of kinetic and static friction was also introduced during this time. Coulomb discovered that the initial friction increases during the time of stationary contact between surfaces and used this mechanism to explain the general observation that static friction is higher than kinetic friction (Scholz, 2002). He also proposed a law (Coulomb's law of friction) stating that kinetic friction is independent of the sliding velocity. These classic theories of friction were able to explain the concept of friction, but failed to account for frictional wear and energy dissipation through friction. In the last century, research has been focused on understanding the physical mechanisms behind friction. The modern concept of friction is generally attributed to Bowden and Taylor (1950, 1964) who introduced an adhesion theory for friction, which is based on the concept of asperities (fig. 3) and the real area of contact created by asperities that touch each other. The real area of contact A_r is generally much smaller than the geometric area of the surface between two bodies (Bowden & Tabor, 1950; Bowden & Tabor, 1964). Bowden and Taylor (1950, 1964) assumed that the normal load N determines the real area of contact:

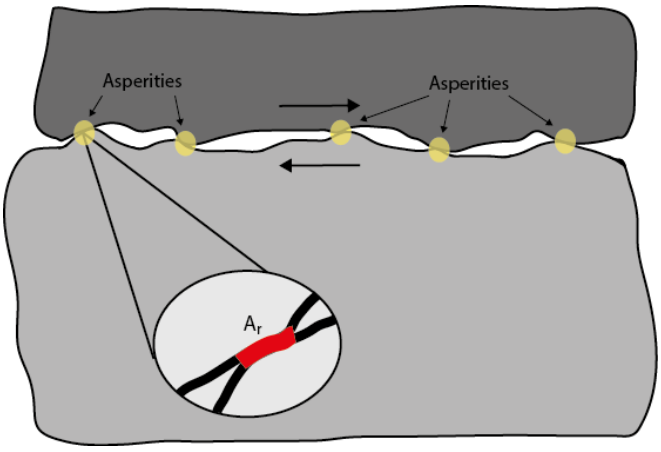

Figure 3 Schematic representation of a contact surface showing several asperities. A_r shows the real area of contact created by one asperity.

$$N = pA_r \quad (1)$$

Where p is the penetration hardness, which is a measure for the strength of a material. Because of the relative small area of contact and the load it is exposed to Bowden and Taylor (1950, 1964) assumed adhesion occurs between the contact areas of asperities. For two bodies to be able to slip the asperities would have to be sheared through, which occurs when the frictional force F is equal to the sum of the shear strength of A_r of the asperities.

$$F = sA_r \quad (2)$$

Where s is the shear strength of the material. Combining the two equations gives the coefficient of friction μ, as $\frac{F}{N} = \frac{p}{S}$, which describes friction. These equations explain the mechanisms behind the friction laws proposed by Amontons. However, the theory of adhesion in itself is not sufficient enough to fully describe friction. Other processes such as asperity ploughing, riding up, interlocking and the effect of fault gouge also have an influence on the coefficient of friction.

Friction is an important variable that influences the characteristics of an earthquake. Stick-slip behavior is considered to be the laboratory equivalent of the seismic cycle (Brace & Byerlee, 1966;

Byerlee, 1970). The alternation between motion and non-motion that describes stick-slip motion is also an alternation between static and kinetic friction. Since static friction exceeds kinetic friction a healing mechanism has to exist which restores the static friction after slip occurs. In 1951, Rabinowicz proved that such a healing mechanism exists. He showed that μ_s increases approximately as log t, when two surfaces are held in stationary contact under load for a time t. Rabinowicz furthermore observed that in order for friction to change to the dynamic value, a critical slip distance D_c has to be overcome. D_c is interpreted to represent to the mean diameter of the contact junction (Rabinowicz, 1956), therefore linking D_c to the grain size when using spherical particles as the friction volume. A combination of all these criteria leads to the following equation, which describes when slip instability occurs (Scholz, 1990):

$$\frac{(\mu_s-\mu_d)\sigma_n}{D_c} > k \qquad (3)$$

Where k is the spring stiffness. Equation 3 shows that instability can only occur when the friction drop is large enough and occurs fast enough, otherwise healing would arrest slip.

Application of velocity dependent friction combined with the healing mechanism to rock friction was first done by Dieterich (1972) and (Scholz et al., 1972). The first one to report on the significance of the velocity dependency of friction was Ruina (1983). He showed that when a slip instability occurs in a velocity strengthening system, any unstable motion will quickly return to a state of stable sliding. A velocity weakening system will, however, always turn an unstable motion into growing oscillations until a state of regular stick-slip is reached (Scholz, 1990). Without velocity weakening, the healing mechanism can create slip instabilities if the condition of equation 3 is met, but it will not result in regular stick-slip. When subjecting a sliding system to a sudden increase in velocity, i.e. a velocity step, an immediate increase in friction occurs (the direct effect) followed by a decrease in friction to a new steady state value (the evolution effect) (fig. 4), where the dynamic friction depends logarithmically on sliding velocity. These observations were made by Dieterich (1979) who fit them to an empirical constitutive law. In 1983, Ruina translated this empirical constitutive law into a rate and state dependent friction formulation. A modern adaption of the constitutive law, based on the connection between time and velocity dependence, is defined for both laws proposed by Ruina and Dieterich:

$$\mu = \mu_0 + a\ln\left(\frac{V}{V_0}\right) + b\ln\left(\frac{V_0\theta}{D_c}\right), \qquad (4)$$

where μ_0 is the reference coefficient of friction for steady state slip at velocity V_0, V is the friction slip rate and a and b are empirical constants. The state variable θ was introduced by Ruina (1983) and can be substituted into Dieterich's original law.

The fundamental differences between the constitutive laws proposed by Dieterich and Ruina lie in the evolution of the state variable, which is described by a second law. Dieterich (1979) stressed the importance of contact time, were the effective contact time is given by the ratio between the critical slip distance D_c and the slip velocity V. Here, D_c is believed to be the slip distance needed to renew the surface contacts and thus defines an average contact lifetime θ

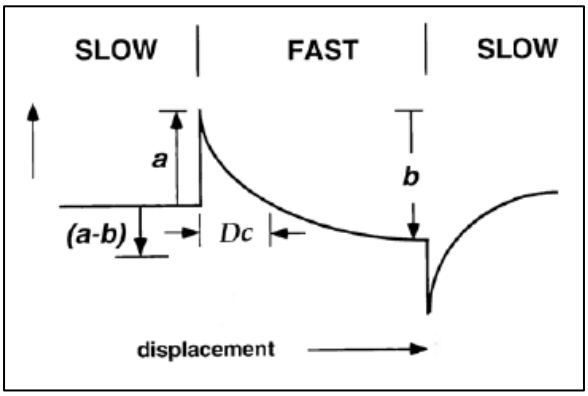

Figure 4 Response of friction on a sudden increase and decrease in velocity and definition of the RSF constants.(Scholz, 1990)

(Marone, 1998).

The resulting evolution law is also known as the aging law:

$$\frac{d\theta}{dt} = 1 - \frac{V\theta}{D_c} \quad (5)$$

Ruina proposed a different evolution law, known as the slip law, which stressed the importance of velocity and slip, rather than time:

$$\frac{d\theta}{dt} = -\frac{V\theta}{D_c} log\left(\frac{V\theta}{D_c}\right) \quad (6)$$

The slip law states that any change of friction requires slip including strengthening during quasistatic contact (Marone, 1998).

3. Methods

3.1.1 Experimental setup

To simulate slip in a laboratory environment a variety of experimental configurations can be used. For this study, a simple spring-slider system is used (fig. 2). The base surface consists of a smooth marble slab with a length of 40 cm and a width of 6.8 cm. To be able to produce events with similar stress drops and displacements a layer of glass beads is placed on the marble surface over which the slider block is pulled. A number of different glass beads sizes have been used which all have a maximum particle distribution no larger than 100 µm. The slider block is made of polyoxymethyleen with a contact surface area of 12.4 by 6.5 cm and a beveled edge to limit the accumulation of glass beads at the leading edge. The spring is pulled at a constant speed by a gearbox connected to an electro motor, which can achieve a maximum load point velocity of 6.24 mm/s. A load cell is placed between the slider block and the spring to measure the force exerted on the block. The displacement is measured using a displacement sensor that is attached to back of the slider block. To achieve a constant layer thickness a custom made tool is used to facilitate leveling the glass beads layers to different thicknesses. The thickness of the layer is taken at a minimum of 5 times the grain diameter.

3.1.2 *Variable input conditions*

To investigate the effects of normal load F_n, load point velocity $V_{load\ point}$, spring stiffness k_{spring} and grain size on the displacement, force drop dF and maximum velocity Vmax of stick-slip events, a range of experiments were done with varying parameters. The various input conditions used for each experiment are shown in table 1. Different normal loads were achieved by adding weights on top of the slider block.

Input conditions	Values
F_n (N)	24.351; 28.273; 32.201; 36.124; 41.430
$V_{load\ point}$ (m/s	$6.24*10^{-3}$; $6.24*10^{-4}$; $2.496*10^{-4}$; $1.248*10^{-4}$; $6.24*10^{-5}$
k_{spring} (N/m)	227.65; 540; 895.5
Grain size (µm)	100-140; 150-210; 300-400; 400-500

Table 1 Values of the parameters used in the experiments and in the numerical model

3.1.3 Sensors, data collection and data processing

Two variables are measured during the duration of an experiment. The load cell measures the force exerted on the slider block, while the displacement sensor measures the displacement of the slider block. The load cell used is an *Omegadyne* LCMFL-20N subminiature load cell capable of measuring forces up to 20N. It is connected to a signal conditioning box with an *Omega* DP25B strain gage panel meter that displays the voltage during an experiment. The displacement sensor is custom made by the HPT technician E. de Graaff and records the displacement of the slider block through the unwinding of a cylinder connected to a potentiometer. It records the signal in volts and transfers it to a second signal conditioning box that displays the voltage during an experiment. The output of both sensors is in voltage and thus prior to use, both sensors were calibrated. Calibration of the load cell was done by measuring the output voltage while varying the force exerted on the load cell by suspending brass weights under the load cell (Appendix A, 1-4). The brass weights were weighed on a digital scale with a resolution of 0.01 gram. The potentiometer was calibrated by measuring the output voltage while varying the displacement (Appendix A, 5). The displacement was measured from a fixed point using a digital caliper with a resolution of 0.01 mm. The load cell was calibrated three more times in between experiments (Appendix A, 2-4), because of its sensitive nature. Due to processing of the acquired load cell data by the conditioning box, a delay of about 0.5 seconds is present between the displacement measured by the speed sensor and the force drop measured by the load cell.

After the signals from the load cell and displacement sensor have been conditioned, the analogue signals are sent to a *TiePie Handyscope HS5-530XM* digital oscilloscope capable of sampling up to $500*10^6$ samples per second. To keep down file size whilst maintaining enough data density to obtain a representative data set, the sampling speed is set at 10000 samples per second with a 16 bits A/D conversion, resulting in 0.244 mV digital resolution with a maximum range of 10 V. The oscilloscope is connected to a computer where *TiePie Multi Channel* software processes and displays the collected data and, when required, stores data to disk. Data can be stored in different data file formats. For further processing the data is stored in a CSV (Comma Separated Values) file.

Data analysis is done using a graphical analysis program called *Xlook*. To be able to use the acquired data the first nine rows of the CSV file, containing information about *TiePie*, are replaced by a header:

Time	*Force*	*Displacement*
s	*V*	*V*

The resulting file is then converted to a look format binary file which can be opened in *Xlook*. Data analysis is done by manually measuring the dt, dx, dF, and Vmax of every slip event in *Xlook* and processing the results in *Microsoft Excel*. *Kaleidagraph* is used to make graphical representations of the acquired data. To determine the velocity of the sliding block and reduce the noise of the displacement sensor the 'running average slope' (RAS) of the displacement data is calculated. This calculation technique takes the average slope over an x amount of data points on each side of the data point over which the RAS is calculated. A variety of different data point ranges was used to determine the most representative velocity curve in most cases, 250 data points on each side was found to be an adequate window size. The friction coefficient is calculated by dividing the peak load force by the normal force (i.e. the weight of the block plus the added weights).

3.1.4 Statistical analysis

Experimental data is often influenced by different factors during the measuring and collecting process. The resulting data is therefore subjected to errors created during the different steps taken to measure, record and analyze the data. Reduction of the error margin is done by repeated calibration of the measurement equipment, careful recreation of the initial conditions, and precise analysis of the data. Since it is impossible to completely eliminate errors in experimental data they have to be taken into account. Of importance to the validity of an experiment is the ability to reproduce results through different experiments. Reproducibility of an experiment is determined by calculating the mean value for the acquired results and its associated standard deviation. The maximum allowable standard deviation is taken at 10% of the mean value for most of the results, but exceptions are made for the force drop dF of the experiments with varying the normal force F_n, due to large standard deviations for this parameter while the other variables do not exceed 10% standard deviation. The standard deviation of the recurrence time is not taken as a criteria for determining outliers because of the smaller sample size, which is caused by the removal of outliers from the data set based on the other variables. This leads to irregular timing of registered slip events and therefore recurrence times that do not represent the actual data. Outliers are identified and eliminated on the basis of a large standard deviation or when they can clearly be identified as irregular slip events. The typical amount of outliers per experiment range between 1 per 5 to 10 events including all of the recorded stick-slips. During the collection and analyses of the spring slider data several factors contribute to the error value, including: the thickness of the glass beads layer; the determination of dt, dx, dF, and Vmax through Xlook (which is done by hand); the correct placement of the (weight on the) slider block; the atmospheric conditions in the lab room; and the sensitivity of the measuring equipment.

To confirm the validity of the collected data, a statistical analysis is performed by creating histograms of each experimental data set after removing the outliers. The bin size of the histograms is calculated using the Freedman-Diaconis (1981) rule, which is based on the interquartile range:

$$x = 2(IQR)n^{1/3} \quad (7)$$

Where x is the bin width, IQR is the interquartile range, and n is the number of data points. The interquartile range is the difference between the first quartile (25%) and the third quartile (75%) of the data set. The Freedman-Diaconis rule is a robust method for determining the bin size of a density histogram and can be used in a wide variety of cases. Due to the usage of the interquartile range this method is less sensitive to outlying data points.

3.1.5 F*rictional volume*

The fault gouge is composed of a layer of glass beads resting on the marble surface and is leveled by sliding a custom-made tool with a flat surface across the sliding surface. No effort was made to arrange the glass beads in any special way. To create a friction surface with constant frictional properties that produce events with a constant amount of slip, glass beads with a maximum particle size distribution of 100 µm were used. Figure 2a shows the glass beads, with a size ranging between 300-400 µm, prior to usage. Notable are the angular elongated particles, small 'glued' together glass beads and the very small glass beads that are regularly present in the glass beads samples. All of these irregular objects interfere with the homogeneity of the friction layer and affect µ, hence also affecting the error margin of the experiments. Figure 2b and 2c show the same glass beads when they have been used for stick slip experiments. There are no signs of wear found on any of the glass beads that were used in the experiments (figure 2c).

3.1.6 Ottawa sand experiments

Additional experiments were performed using Ottawa sand as the friction layer. Figure 2d shows the Ottawa sand used in the experiments. The sand size ranges from 425-500 µm and has a sub-angular shape. The sand consists for 99.7% of silica dioxide and is obtained from the U.S. Silica Company, Ottawa, Illinois and has been used in previous laboratory studies (Mair & Marone, 1999; Mair et al., 2002). Due to the small applied F_n and the smooth surface of the polyoxymethyleen slider block no stick-slip events could be created. Instead the experiments resulted in stable sliding of the slider block. To achieve better results a sandstone slider block with a contact surface of 10.1 cm by 6.7 cm was used. The sandstone originates from the Bentheim formation and has a porosity of 24.5%, a homogeneous mineralogy and a grain size ranging between 200 µm and 600 µm (Louis et al., 2003). The rest of the experimental setup remained unchanged.

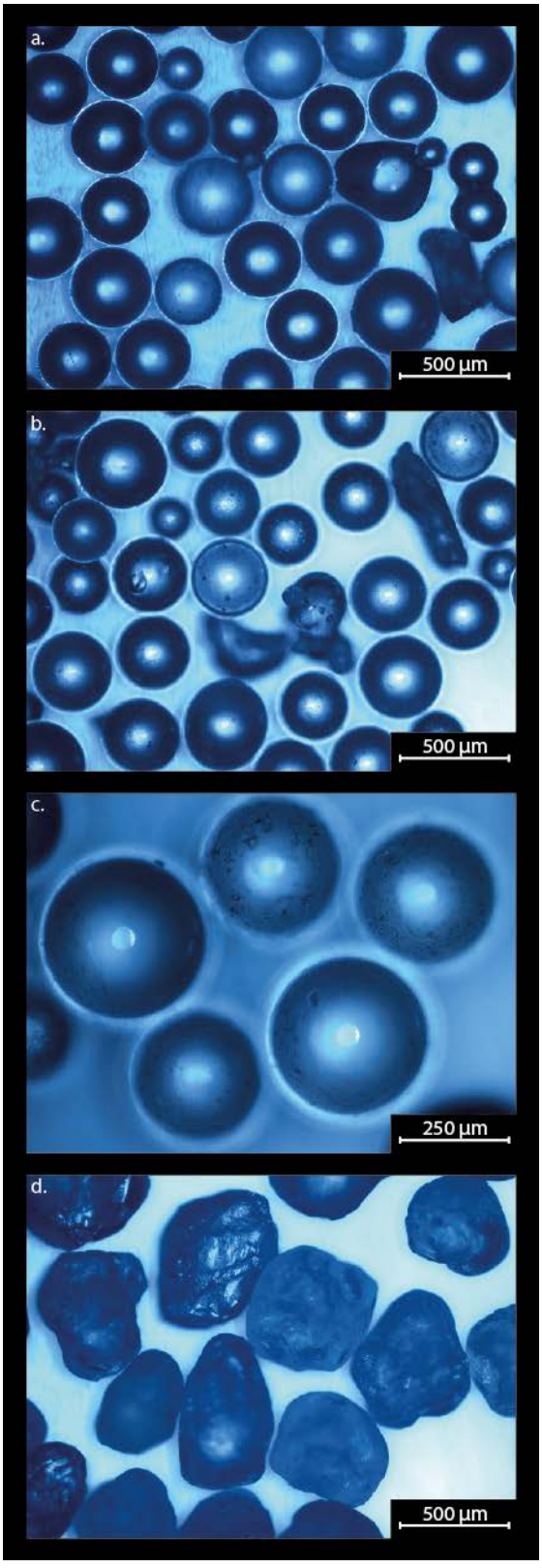

Figure 5 LiDAR images of the glass beads and quartz sand. a) 300-400 µm glass beads before use. b) 300-400 µm glass beads after use. c) Close up of 300-400 µm glass beads. d) Ottawa sand, sub angular, 425-500 µm.

3.2.1 Numerical Model

Being able to simulate an earthquake is one of the essential steps needed to be able to predict the magnitude of an earthquake. Numerous numerical models (Carlson & Langer, 1989; Dieterich, 1986; Hori et al., 2004; Rundle & Jackson, 1977) have been created to simulate the occurrence of earthquake events and with increasing success. One of these numerical models is QDYN, a quasi-dynamic earthquake cycle simulation model, developed by the seismological laboratory of the California Institute of Technology. QDYN is a versatile model due to its extensive features and can be applied to a wide range of different seismological situations. The model is based on rate-and-state friction and is capable of 1D, 2D and 3D simulations. For this study, the 1D spring block simulation is used as an analog for the experimental setup.

Input parameters QDYN	Values
– Spring stiffness	Variable
– Shear wave velocity	10
– a	0.01
– b	0.010045
– Dc	1e-6
– Evolution law for the state variable (aging or slip law)	Aging law
– Effective normal stress	Variable
– Reference steady state friction coefficient	0.4
– Reference steady-state slip velocity	Variable
– Total simulation time	100 s

Table 2 Input parameters and constants used in QDYN.

QDYN is based on a program structure that systematically calculates the different variables per time step and changes the length of the time step depending on the new slip rate. The input parameters that can be used vary per mode (1D, 2D, 3D). In case of a spring-block system the parameters listed in table 3 are used. After running a number of simulations, it became clear that due to the polymer slider block and the scale of the parameter values (o.a. the low normal load) used in the experiments, the shear wave velocity had to be very low at 10 m/s. In comparison, the shear wave velocity when modelling a natural event is often taken at 3000 m/s. The total simulation time is set to 200 seconds consisting of two cycles. The first cycle is a warm-up cycle to erase the effects of the initial conditions. A *Matlab* wrapper is used to provide QDYN with the input parameters (table 2. .

3.2.2 Quasi-dynamic vs. fully dynamic

QDYN stands for Quasi DYNamic earthquake simulator. In a quasi-dynamic (QD) model, the wave mediated stress transfers are ignored and a radiation damping term is used to account for the inertial effects during simulated earthquakes (Thomas et al., 2014). The alternative is the use of fully dynamic (FD) earthquake simulations, which account for full inertial effects during seismic events. However, due to the wide range of temporal and spatial scales involved, this is computationally very challenging (Lapusta, 2000). One of the advantages of using a QD simulation over a FD simulation is the significantly lower computational cost and memory usage.

3.2.3 Calculations

The equation of motion is an integral part of the model and gives the shear stress applied by the spring (eq. 7).

$$\tau_{spring} = -zV - k(dx - dx_{load}) \quad (8)$$

Where τ is the shear stress, z is the impedance, V is the sliding velocity of the slider block, k is the stiffness, dx is the displacement of the block, and dx_{load} is the load displacement of the spring.
The friction is calculated using the rate-and-state-law introduced by Dieterich and Ruina (eq. 4):

$$\tau_{friction} = \sigma_n \left(\mu^* - alog\left(\frac{V^*}{V}\right) + blog\left(\frac{\theta}{\theta^*}\right)\right) \quad (9)$$

Where σ_n (Pa) is the normal stress, μ^* is the reference coefficient of friction, a and b are the rate-and-state parameters, V^* (ms^{-1}) is the reference velocity (i.e. the load point velocity), and θ is the state variable. σ_n, μ^*, a, b, and V^* are fixed input parameters. V at t=0 is the perturbation velocity that is applied at t=0. Both the state variable and the sliding velocity of the block will evolve in subsequent steps. θ^* is the reference state variable and is initialized as:

$$\theta^* = \frac{D_c}{V^*} \tag{10}$$

Where D_c (m) is the critical slip distance.
The stiffness is initialized as:

$$k = G/L \tag{11}$$

Where G is the shear modulus (Pa) and L (m) is the length of the block. The model computation involves three steps. During the first step the shear stress rate (of τ_{spring}) is computed for the next time step:

$$\frac{d\tau}{dt} = -k(V - V^*) \tag{12}$$

The second step sets the time derivatives of τ_{spring} and $\tau_{friction}$ equal and solves equation 13 for V and θ in the Runge-Kutta ODE solver.

$$\frac{dV}{dt} = \frac{\left(\frac{d\tau}{dt} - \sigma_n b \frac{d\theta_1}{dt\theta}\right)}{\frac{\sigma_n a}{V} + z} \tag{13}$$

When substituting dτ/dt in this equation, this gives:

$$k(V - V^*) + z\frac{dV}{dt} = -\sigma_n\left(\frac{a}{V}\frac{dV}{dt} + b\frac{1}{\theta}\frac{d\theta}{dt}\right) \tag{14}$$

The state variable θ is dependent on the state law used. Both the aging law (eq. 5) and the slip law (eq. 6) can be used in the model. The radiation damping term that makes the model quasi-dynamic is called the impedance and is defined as:

$$z = G/2V_s \tag{15}$$

Where G(Pa) is the shear modulus and V_s is the shear wave velocity. During the third step the time step is updated, depending on the new slip rate. After the new V and θ are computed, they are inserted back into the rate-and-state friction equation to compute the new $\tau_{friction}$ and the slip. This process then starts over at step one until the run time is over.

3.2.4 Optimization of a, b and D_c

The rate-and-state friction law is based on a number of RSF parameters (a, b, and D_c). These parameters are typically experimentally determined by performing velocity step tests. However, in the case of glass beads, these (material) constants are not known because in normal sliding experiments, glass beads stick-slip, making it difficult to determine a, b and D_c. To determine a, b and D_c for our glass beads, data produced by QDYN is fit to experimental data. By creating a loop in the *Matlab* wrapper of QDYN that runs through a large amount of combinations between a, b and D_c results similar to one particular experiment are selected and these optimized values for a, b and D_c are used in subsequent simulations.

4. Results

4.1 Experimental data

Force and displacement data is collected during each experiment and analysed. A typical force and displacement curve is shown in Fig. 8a. During the sticking periods, the slider block is at rest and the force F increases in time up to a maximum value F_f. When F_f is exceeded by F, the external shear stress causes the glass beads layer to fail and the slider block to start sliding. During the sliding motion F decreases until the slider block sticks again. When assuming there is no damping and friction drops from the initial static value μ_s to a lower dynamic value μ_d during slip the motion of the slider block can be described as (after (Scholz, 2002):

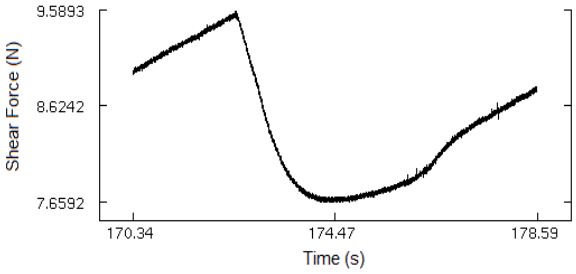

Figure 6 Typical force drop curve

$$ma + kdx = d\mu F_n \tag{16}$$

Where m is the mass and a is the acceleration of the slider block. The slip duration t_r is then given by:

$$t_r = \pi\sqrt{\frac{m}{k}} \tag{17}$$

The slip duration is therefore only dependent on the stiffness and mass and independent of dμ and F_n. The experimental results of t_r compared with equation 17 are comparable (fig. 7). When taking inertial effects into account, equation 17 needs to be modified and t_r is given by (Rice & Tse, 1986):

$$t_r = 2\pi\sqrt{\frac{m}{k}} \tag{18}$$

During the duration of slip the slider block is displaced by a distance dx generating a typical multi-parabolic velocity curve, which is a result of the non-uniform displacement dx of the slider block (fig. 8b). The maximum velocity (Vmax) reached is therefore not the theoretical maximum velocity that can be reached with undisturbed slip. As expected the maximum velocity is reached halfway through the slip event. The force drop curve does not show the same stepwise progression during the slip event (fig. 6). The curve shows a linear decrease during the first part of the slip event after which the slope gradually decreases to zero. During the sticking intervals it is likely that microscopic rearrangements cause some (aseismic) creep to occur. These rearrangements will, increase in frequency when slip is about to occur (Nasuno et al., 1997). However, we did not detect any creep, which means that the creep is either too small to be detected or creep does not occur. In the current

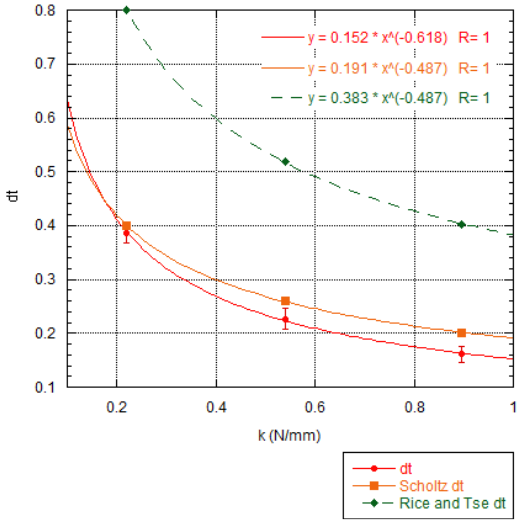

Figure 7 Plot showing the effect of the spring stiffness on the slip duration in comparison with equation 17 and 18.

experimental set-up, the electronic noise typically represents 0.2 mm of displacement implying that possible creep displacement is smaller.

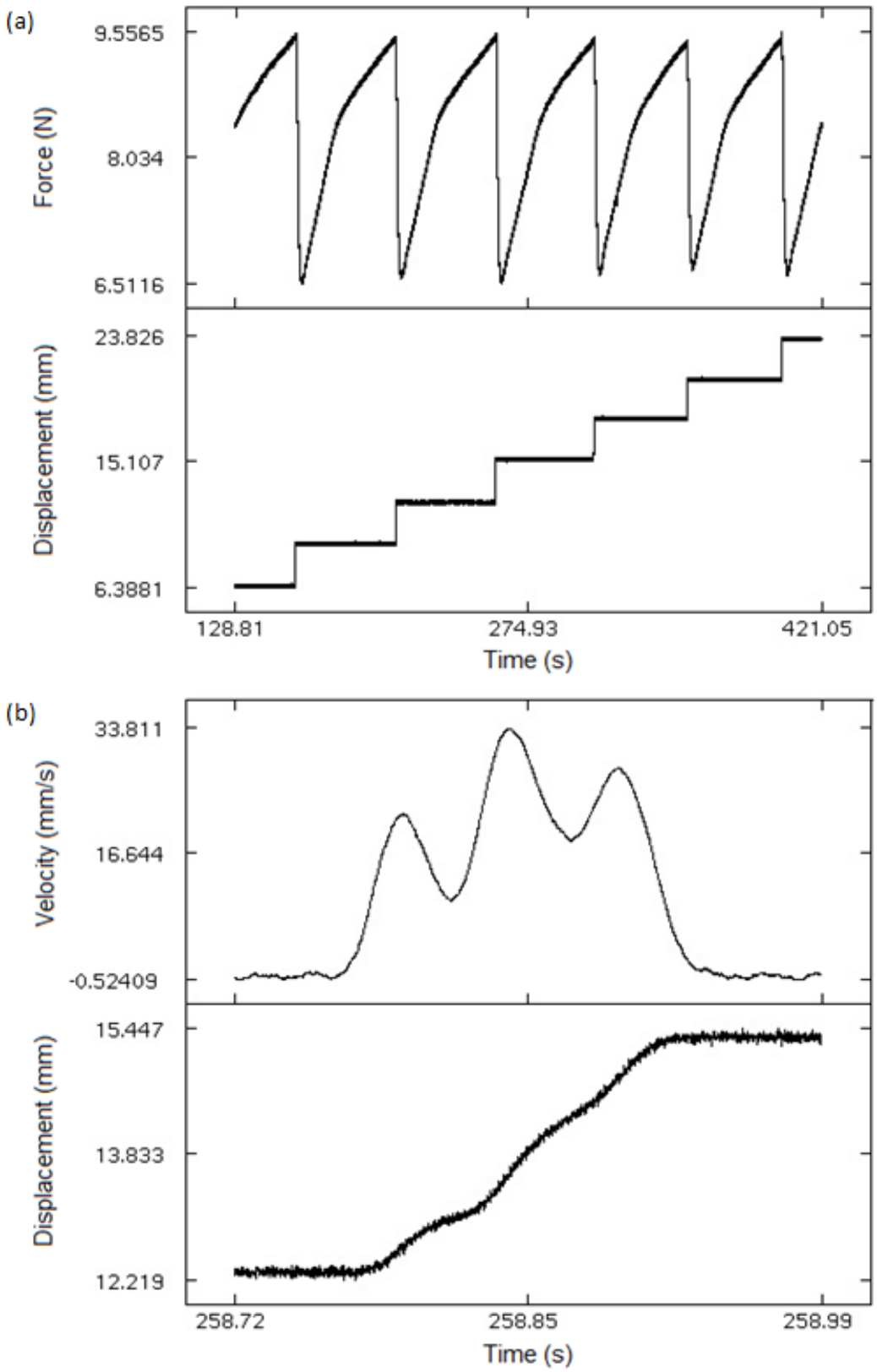

Figure 8 a) Plots showing the force and displacement curve of a series of stick-slip events. b) Plots showing the velocity curve and the displacement curve of a single event.

Nasuno et al. (1997) reported displacement due to creep being equal to 1% of the displacement of the slip event, which suggests that, with a maximum displacement of 14.367 mm, the largest possible displacement due to creep would be 0.14367 mm which is well under the displacement concealed by the noise.

To determine the validity of the collected data of the measured parameters (dx, dF, and Vmax), each set of experiments is subjected to a statistical analysis. Fig. 5 shows examples of the distribution of the dx data acquired during the $V_{load\ point}$ experiments. It is noted that a decrease in $V_{load\ point}$ results in a increase in the quality of the data. For every set of experiments, the shape of the histogram is taken into consideration when evaluating the data. The number of slip events per experimental configuration varies between 50 and 80 events (table 4.). The effects of varying the normal load (F_n), load point velocity ($V_{load\ point}$), grain size and spring stiffness (k_{spring}) on the characteristics of the slip event are determined and table 3 shows the parameters for each set of conducted experiments. Due to irregular stick slip events at a high $V_{load\ point}$ during the k and grain size experiments, they were performed with a lower $V_{load\ point}$ to maintain consistent stick-slip events.

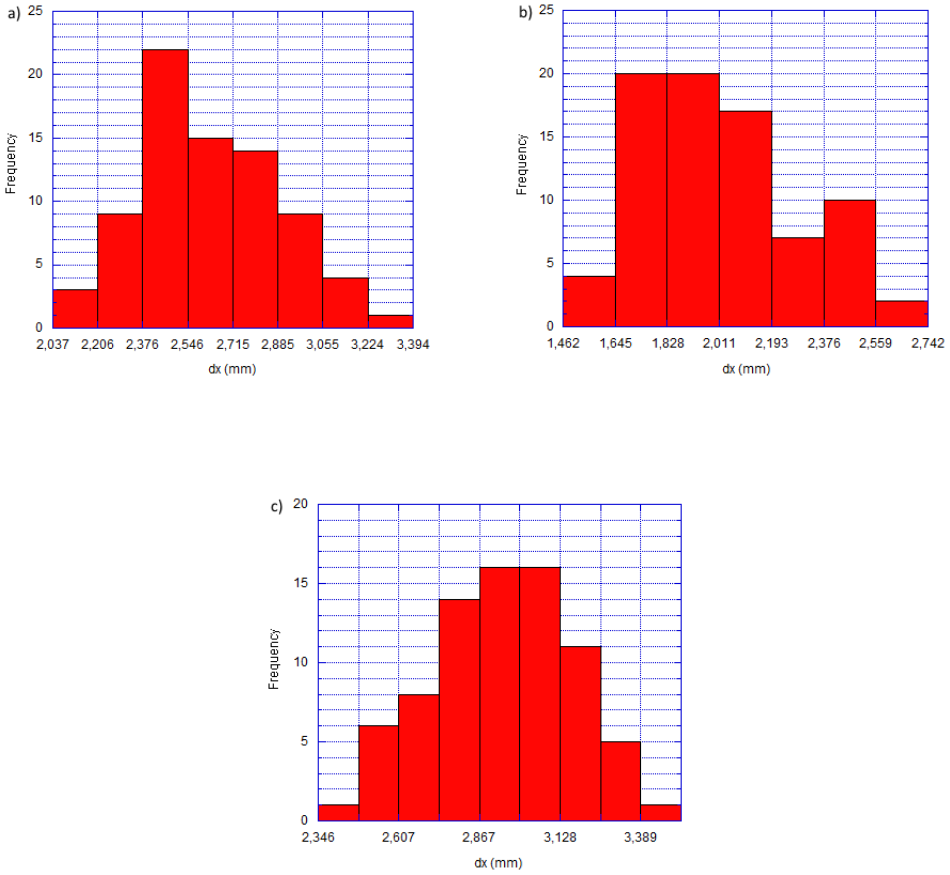

Figure 9 Plots showing data distribution of $V_{load\ point}$ experiments.
a) Representable distribution of dx (Stdev = 0.260 mm, $V_{load\ point}$ = 0.1248 mm/s, F_n = 36.12 N Pa, k = 0.89 N/mm). b) Poor distribution of dx (Stdev = 0.272 mm, $V_{load\ point}$ = 0.2496 mm/s, F_n = 36.12 N, k = 0.89 N/mm). c) Excellent distribution of dx (Stdev = 0.227 mm, $V_{load\ point}$ = 0.0624 mm/s, F_n = 36.12 N, k = 0.89 N/mm).

4.2 QDYN data

The results from QDYN were acquired using the parameters listed in table 3. Because of the use of glass beads as a friction volume, the a, b, D_c and VS values had to be determined by fitting the model data to data acquired from one particular experiment. In addition the effect of (a-b) and D_c on dx, dF

and Vmax while varying the normal load was investigated (fig. 10). The parameters used in QDYN are similar to the parameters used for the glass beads simulations.

From the QDYN simulation data, the following can be concluded. For all variables (i.e. dx, dF and Vmax), the trend with F_n is linear, independent of the size of (a-b) or D_c. An increase in (a-b) results in an increase in both the absolute values and the slope of the dx, dF and Vmax trends. It is observed that changing (a-b) has the most significant effect on Vmax. An increase in D_c results in an increase in the absolute values of dx, dF and Vmax, but does not seem to have a large effect on the slope of the trends observed. The slope for the dx trend is approximately $0.132*F_n$. A variation is present in the slopes of the dF trends in which no general trend behaviour can be observed. The average dF slope is $0.1274*F_n$. The influence of D_c on Vmax is minimal, but a slight decrease in Vmax with an increasing D_c is visible. The average slope for Vmax is $24.3*F_n$.

Variable / Constant	F_n (N)	k_{spring} (N/mm)	$V_{load\ point}$ (mm/s)	Grain size (µm)
F_n	-	0.22765	6.24	150-210
k_{spring} (N/mm)	36.12	-	0.624	150-210
$V_{load\ point}$ (mm/s)	36.12	0.8955	-	150-210
Grain size (µm)	36.12	0.8955	0.1248	-
F_n (Ottawa sand)	-	0.8955	0.1248	425-500

Table 3 Experimental parameters used in the spring slider experiments and QDYN. For each set of experiments one parameter was varied.

4.3 The effect of weight on stick-slip motion

Fig. 4 shows the effect of the normal load on the dx, dF, Vmax and the reoccurrence time in comparison to the results generated by QDYN. Five different loads were used: 24.351, 28.273, 32.202, 36.124 and 41.430 N. The number of slip events analysed varies between 59 and 80. Fig. 11a shows a positive linear relationship between dx and F_n with an outlier present at a dx of 11.91 mm, corresponding to a weight of 32.2 N. Looking at fig. 11a, it is also possible to ignore the two largest F_n points and obtain a linear fit very similar to QDYN.

The Vmax data show a consistent linear relationship between F_n and Vmax. The absolute values of the experimental and QDYN are quite far apart making a comparison between the data set quite hard. However, when disregarding the difference of about 1.5 orders of magnitude between the absolute values a linear trend for both the experimental data and the data from QDYN is visible.

The reoccurrence time graph shows a positive linear relationship between F_n and the reoccurrence time. At F_n = 32.2 the reoccurrence time is slightly higher than expected and the reoccurrence time at F_n = 41.4 N is considered to be unreliable with a standard deviation of 25%.

Plotting dx and Vmax against dF shows a linear increase for both variables consistent with the results of QDYN (fig. 12).

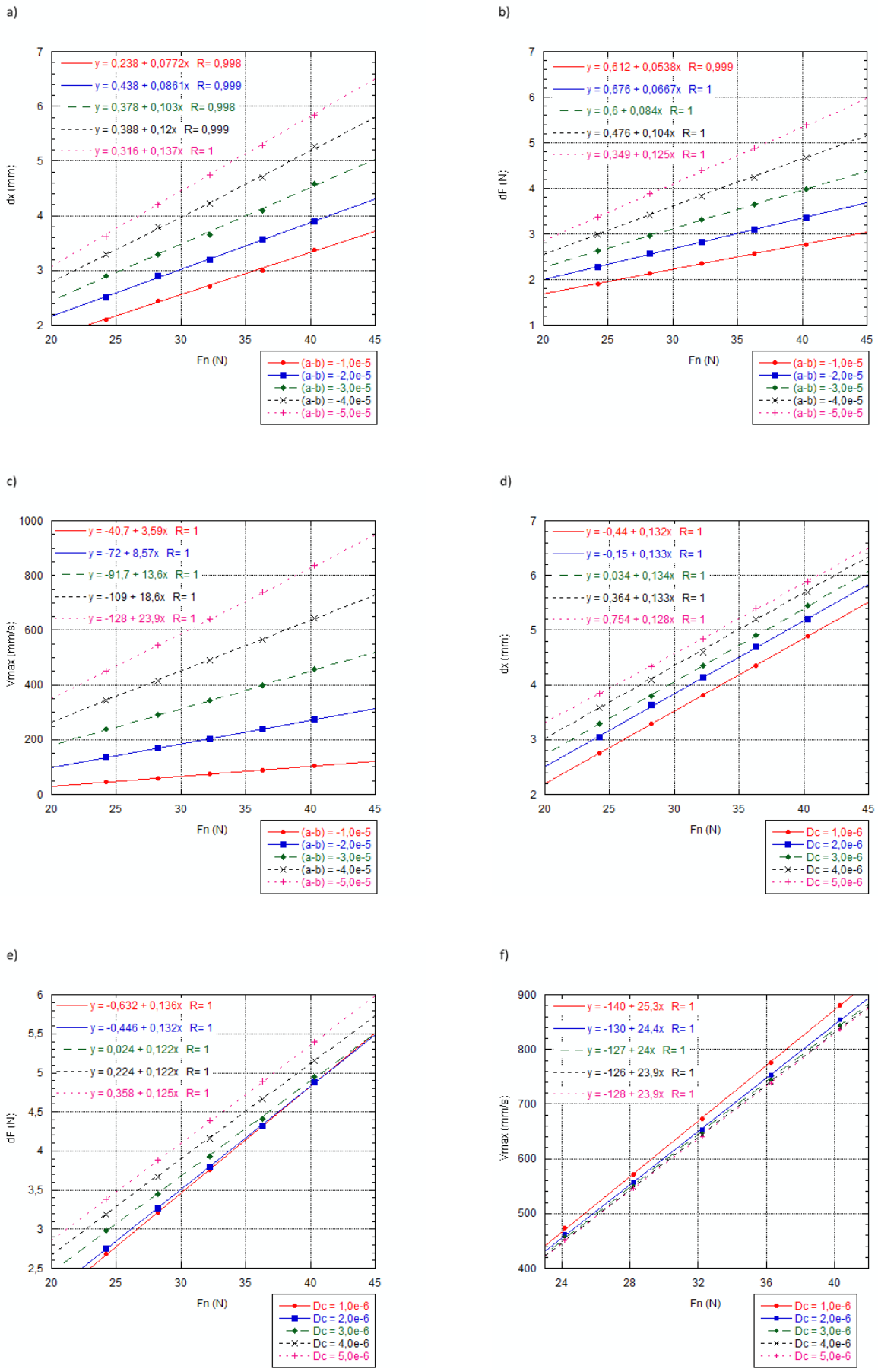

Figure 10 Overview of data acquired through QDYN showing the effect of (a-b) and D_c on displacement, force drop and maximum velocity, while varying the normal load. k = 0.8955 N/mm, $V_{load\ point}$ = 0.624 mm/s. a)The effect of (a-b) on dx. b)The effect of (a-b) on dF. c)The effect of (a-b) on Vmax. d)The effect of D_c on dx. e)The effect of D_c on dF. f) The effect of D_c on Vmax.

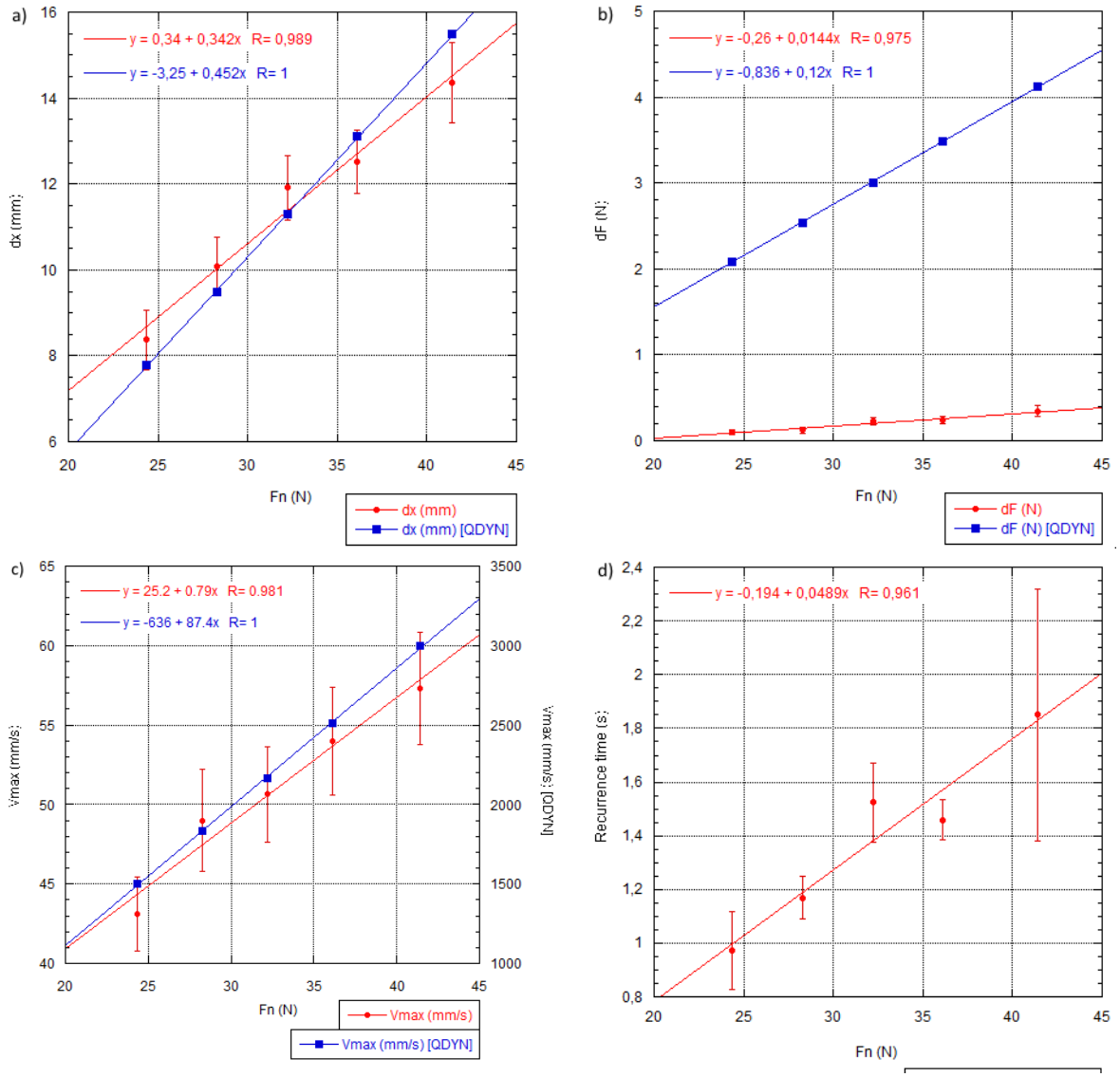

Figure 11 Overview of experimental and QDYN data showing the effect of the normal load on the displacement, force drop, maximum velocity and reoccurrence time. The following parameters where used: k = 0.22765, $V_{load\ point}$ = 6.24 mm/s and grain size = 150-210 µm.

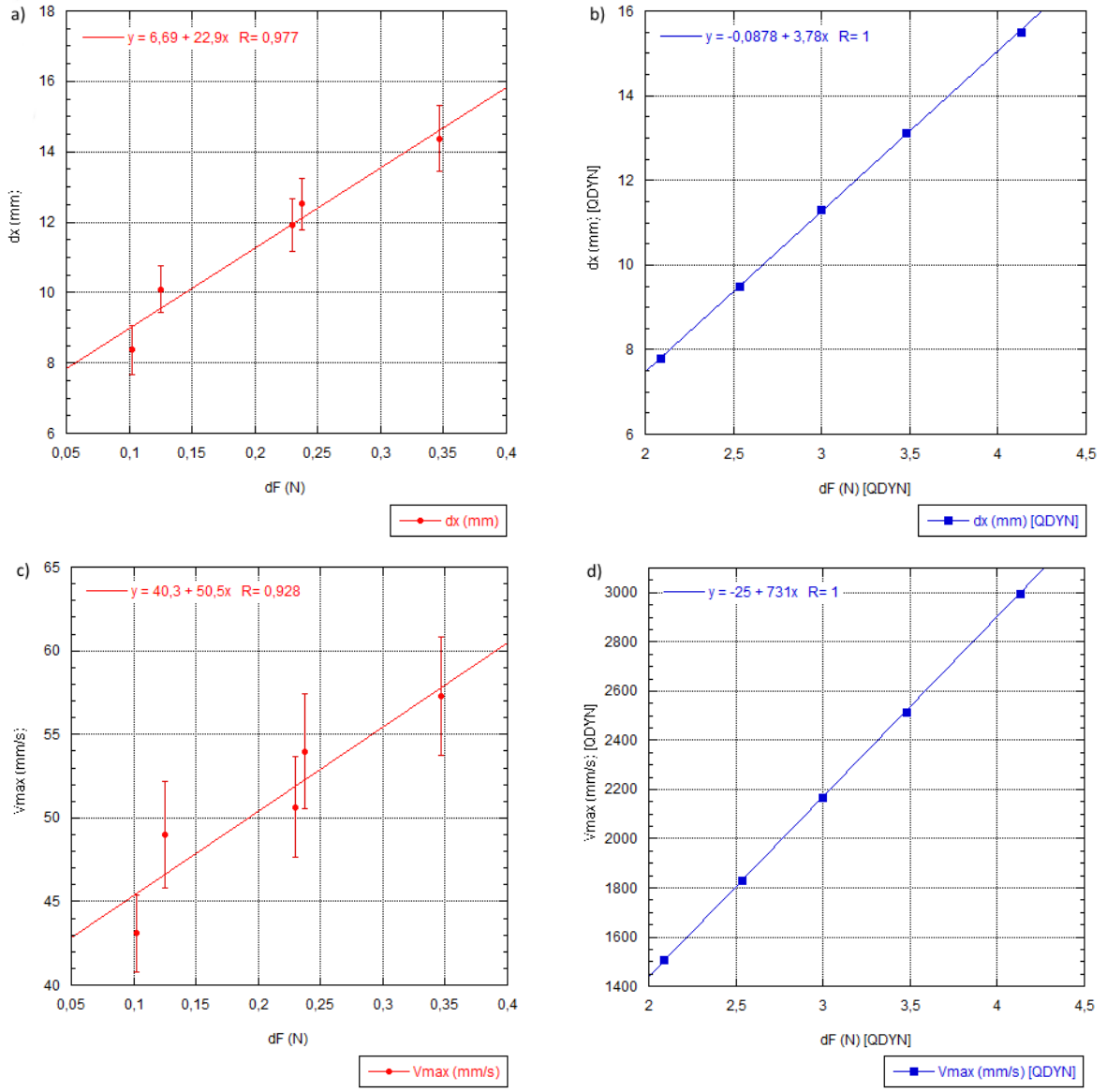

Figure 12 Overview of experimental and QDYN data showing how the displacement and maximum velocity are effected by the force drop when varying the normal load. The following parameters where used: k = 0.22765, $V_{load\ point}$ = 6.24 mm/s and grain size = 150-210 µm.

4.4 The effect of spring stiffness on stick-slip motion

To determine the effect of k_{spring} on dx, dF, Vmax and recurrence time, spring slider experiments were conducted using three springs with spring stiffness's of 0.22, 0.54 and 0.89 N/mm (Appendix B,C). F_n was kept constant at 36.124 N, $V_{load\ point}$ for all experiments was 0.624 mm/s and the grain size of the glass beads used ranged from 160 to 210 µm. Appendix A shows the effect of the spring stiffness k on dx, dF, Vmax in comparison with the results from QDYN and the relation between dF and dx/Vmax. The number of slip events used ranges from 66 to a maximum of 70 slip events per setting.

The general trend identified in this data is that the dependence of the different variables on the spring stiffness follows power laws. A plot of dx and k of both the experimental and QDYN data shows a good fit between the two data sets and although the experimental data itself fits the respective trend well, a better fit with the data from QDYN can be obtained by lowering dx at k = 0.89 N/mm (Appendix B-1).

A similar trend is observed in the relation between k and dF. The data from QDYN fits a negative power law and is also applied to the experimental data. However, at k = 0.89 N/mm the dF does not fit this trend and is expected to be a significantly lower value (Appendix B-2). Overall, the absolute QDYN values are a factor ~3 larger than the experimental measurements.

The experimental and QDYN data both show a negative power law relation between k and Vmax with a large difference in actual values. The reoccurrence time behaves in a similar fashion under a negative power law.

Analysis of the relation between dF and Vmax show that an increase in dF leads to an increase in Vmax as is expected (Appendix C). A positive power law results in the best trend line correlating the two variables. Analysis of the relation between dF and dx shows a similar pattern, but at dF = 2.3, Vmax is lower than expected. This is also shown in the k-dx graph.

4.5 The effect of grain size on stick-slip motion

To determine the effect of the grain size on dx, dF, Vmax and the reoccurrence time, spring slider experiments were conducted with grain sizes: 100-140 µm, 160-210 µm, 300-400 µm and 400-500 µm (appendix D). F_n was kept constant at 36.124 N, the Vpull for all the experiments was constant at 0.1248 mm/s and a k of 0.89 N/mm was used. The number of slip events used ranged between 56 and 77. At a grain size of 100-140 µm the average coefficient of friction was found to be 0.277, which is higher than any other coefficients of friction observed.

The experimental results for the effect of grain size on dx, dF and Vmax show significant scatter and lack a clear dependence of dF and Vmax on the grain size (Appendix D-1,3,5). For dx a negative linear trend is visible similar to the QDYN trend when ignoring the outlier at grain size = 160-210. Because it is not possible to directly use grain size as a parameter in QDYN, D_c is used as it should be related to the real contact area. QDYN results show a negative linear relation when relating D_c to dx and dF. When increasing D_c, Vmax does not increase linearly but by a positive power law. This is contrary to the trend observed between F_n and Vmax, where the other relations were also linear. The experimental data for the reoccurrence time seems to be following a negative power law, but due to the lack of data density, this is not certain.

A linear trend is visible for the increase of dx and Vmax with dF (Appendix E).

4.6 The effect of the load point velocity on stick slip motion

To determine the effect of $V_{load\ point}$ on dx, dF and Vmax spring, slider experiments were conducted with load point velocities of 0.0624, 0.1248, 0.2496 and 0.624 mm/s (appendix F). A normal force of 36.12 N was used in combination with a spring stiffness of 0.89 N/mm. The used grain size ranged between 150-210 µm. The number of slip events per load point velocity was variable between 62 and 80.

Overall, the data shows one outlier at a $V_{load\ point}$ of 0.624 mm/s for all of the variables measured. The results produced by QDYN show logarithmic relationship between $V_{load\ point}$ to dx, dF and Vmax. The experimental dx data shows a negative linear trend, but can also be fitted with a logarithmic trend. The Vmax data shows a more distinct logarithmic trend. The dF data is best fitted with a linear trend.

It is observed that dx and Vmax increase when dF increases (Appendix G). Due to a very limited data set, the recurrence time is not plotted.

4.7 The effect of the normal force on stick slip motion using Ottawa sand as the friction volume

The results using Ottawa sand with a grain size of 425-500 µm as fault gouge where conducted at various F_n: 23.367, 27.289, 31.218 and 35.140 N. $V_{load\ point}$ was set at 0.1248 mm/s and a k of 0.89 N/mm was used. The data acquired from the Ottawa sand experiment show trends similar to the glass beads experiments, but with a larger standard deviation of around 25% (Appendix H). The RSF parameters used in QDYN where adjusted to fit the experimental results: a = 0.01, b = 0.010025, D_c = 0.0000001, VS = 10 and reference steady state friction coefficient = 0.6. An excellent fit was acquired for the dF data with only a small increase in terms of the absolute values. The dx trend produced by QDYN is a factor of two lower than the trend seen in the experimental data. The Vmax results from QDYN are an order of magnitude larger than the experimental results, but they both show a linear trend. The reoccurrence time increases linearly with F_n. An increase in dF leads to an increase in dx and Vmax (Appendix I).

4.8 Average coefficient of friction

The average peak coefficient of friction is relatively consistent for all the performed experiments at µ = 0.239. The F_n experiments have an average µ of 0.254, which is slightly larger than the other glass beads experiments and the experiments with grain size of 100-140 have an outlier of µ = 0.278. As expected, the experiments conducted using the Ottawa sand as a friction surface and a sandstone slider block have a larger average peak coefficient of friction at µ = 0.356. An increase in both the k_{spring} and the $V_{load\ point}$ gives a slight increase in µ.

Variable	Value	# of slip events	dx (mm)	Stdev dx (mm)	dx QDYN (mm)	dF (N)	Stdev dF (N)	dF QDYN (N)	Vmax (mm/s)	Stdev Vmax (mm/s)	Vmax QDYN (mm/s)	Reocc. time (s)	Stdev Reocc. time (s)	Average μ	k_{setup} (N/mm) Hooke's Law/spring k (N/mm)	
F_n (N)	24.351	68	8.368	0.692	7.8	0.102	0.0284	2.09	43.102	2.320	1504.1	0.971	0.145	0.255	0,012	0.2369
	28.273	80	10.088	0.664	9.5	0.124	0.0346	2.54	48.989	3.208	1830.7	1.169	0.078	0.251	0,012	
	32.202	62	11.915	0.752	11.3	0.229	0.0442	3	50.648	2.997	2168.4	1.524	0.147	0.248	0,019	
	36.124	60	12.513	0.733	13.1	0.237	0.0423	3.48	53.988	3.411	2514.7	1.459	0.073	0.250	0,019	
	41.430	59	14.367	0.934	15.5	0.347	0.0662	4.13	57.294	3.527	2996.2	1.851	0.469	0.266	0,024	
k_{spring} (N/mm)	0.2277	70	13.936	0.624	18.37	2.314	0.105	4.77	58.716	3.032	3464	21.257	1.1799	0.229	0.167	0.2277
	0.54	66	5.258	0.237	6.81	1.724	0.087	4.13	42.376	3.291	1243.4	7.9111	0.31267	0.233	0.328	0.54
	0.8955	69	4.068	0.282	4.05	2.062	0.139	3.79	42.706	2.580	676.6	5.9711	0.48707	0.238	0.508	0.8955
$V_{Load\ point}$ (mm/s)	0.0624	78	2.937	0.227	5.4	2.867	0.162	5.08	34.975	3.148	914.9	-	-	0.217	0.979	0.8955
	0.1248	77	2.624	0.260	5	2.116	0.116	4.7	33.840	2.288	846.1	-	-	0.224	0.811	
	0.2496	80	2.005	0.272	4.6	1.322	0.132	4.32	26.413	1.987	775.1	7.2236	0.69042	0.228	0.663	
	0.624	62	4.042	0.282	3.96	2.077	0.138	3.79	42.794	2.642	676.6	5.9876	0.66831	0.238	0.515	
Grain size (μm) Dc	100-140 1e-06	57	6.246	0.676	6.45	3.143	0.210	5.19	47.278	4.684	754.7	49.257	4.812	0.278	0,507	0.8955
	160-210 2e-06	77	2.625	0.260	6	2.116	0.116	4.93	33.840	2.288	755.6	-	-	0.224	0,811	
	300-400 3e-06	56	5.158	0.419	5.55	3.464	0.142	4.65	45.995	2.070	757.2	40.854	2.155	0.233	0,676	
	400-500 4e-06	70	2.973	0.241	5.1	3.117	0.225	4.39	36.695	2.973	761.1	23.481	1.522	0.214	1,035	
	- 5e-06	-	-	-	4.65	-	-	4.32	-	-	775.1	-	-	-	-	
F_n (N) Ottawa sand	23.367	84	1.831	0.602	1.79	0.945	0.381	1.85	23.510	5.142	340.8	13.157	0.356	0.356	0.509	0.8955
	27.289	76	3.325	0.647	2.15	1.305	0.318	2.23	30.591	4.059	409.8	24.571	0.352	0.352	0.389	
	31.218	70	4.212	0.703	2.52	1.684	0.294	2.61	33.738	3.724	480.7	31.267	0.350	0.350	0.401	
	35.140	70	4.759	0.775	2.89	1.946	0.349	3	36.520	4.459	552.8	35.822	0.365	0.365	0.412	

Table 4 Experimental results for all 5 sets of experiments performed

5. Discussion

5.1 Peak friction

The peak friction of the gouge layer is relatively consistent for each set of experiments. Two observations are made on the peak friction of the different sets of experiments: there are slightly larger peak frictions during the F_n experiments and an outlier ($\mu = 0.278$) is present at a grain size of 100-140 μm (table 4). The first observation can be explained by the low dF values during the F_n experiments. The unusually low dF, in comparison to the other experimental results, results in a μ with a slightly higher value. The second observation is related to the scattered data distribution, and consequently, the reliability of the grain size experiments.

In comparison to other work the total average peak friction ($\mu = 0.239$) using glass beads and a smooth surface is higher than expected. Anthony and Marone (2005) reported a μ of ~0.12 using mirror-finished hardened steel as a smooth friction surface and a μ of ~0.45 using a surface with triangular grooves of 0.8 mm deep, spaced 1 mm apart as a roughened friction surface. They conducted their experiments with a double direct shear testing apparatus at normal stresses of 5 and 10 MPa with loading velocities ranging from 0.1 to 300 μm/s (Anthony & Marone, 2005). The spherical fault gouge consisted of 105-149 μm glass beads (Anthony & Marone, 2005). It is important to note that under these conditions the gouge sheared between the smooth surfaces always exhibited stable sliding as opposed the unstable stick-slip behavior exhibited when the gouge was sheared between rough surfaces (Anthony & Marone, 2005). More recently it was found that the transition between rolling and jamming in granular layers occurs at $\mu = \sim 0.12$ (Marone et al., 2008). The total average peak friction ($\mu = 0.239$) observed in this study does not correspond to the smooth surface results of Anthony and Marone. It can be assumed that the smooth surface of the slider block and the underlying slab are not as smooth as the mirror finished hardened steel and therefore increase μ. Furthermore, additional effects such as accumulation of glass beads between the sidewalls and the slider block can also result in an increase in μ. The k_{spring} and $V_{load\ point}$ data show an increase of μ with an increase of k_{spring} and $V_{load\ point}$, but due to the relatively small increase no definitive conclusion can be drawn on the velocity and stiffness dependence of μ.

The Ottawa sand experiments show a consistent average peak friction ($\mu = 0.356$), which is lower than the quartz sand results from Anthony and Marone (2005) who reported a μ of 0.57 using a rough friction surface and the same Ottawa sand with a size ranging from 50 to 150 μm. The average peak friction does correspond with the glass beads results from Anthony and Marone. This difference is largely explained by the marble slab used as the underlying friction surface for the Ottawa sand experiments, which results in only on rough surface affecting the coefficient of friction in comparison to the two rough surface used by Anthony and Marone. Additionally, the rough surface used by Anthony and Marone is different from the rough sandstone surface used during the Ottawa sand experiments. The observation that for both friction volumes the friction is different from the friction values found by Anthony and Marone can be explained by the used friction surface during our experiments. The polymer slider block is not as smooth as the mirror-finished hardened steel and, therefore, provides more friction. The marble slab and sandstone slider block are not as rough as the two friction surfaces, used by Anthony and Marone, combined

5.2 Evolution of friction (shear force) with load-point displacement (time)

The loading curves of the experiments show a two stage pattern (fig. 6a). The initial increase of the force exerted on the slider block has a steep slope which decreases after a certain period of time depending on the stiffness of the spring k_{spring}. A large k_{spring} increases the time before the slope of the exerted force decreases. This variance in the stiffness of the experimental setup k_{setup} during stick is not expected and is an indication that k_{setup} is influenced by other components of the experimental setup that become important after a certain threshold force is exceeded. Theoretically k_{setup} is determined by k_{spring}, due to the infinitely high stiffness of the other components influencing k_{setup}. Analysis of the dx and dF curves of a number of slip events under different conditions revealed that in most cases k_{setup} is in fact not equivalent to k_{spring}. The high k_{setup} can be caused by the slider block sliding against the sidewalls or the weights not being placed in the middle of the slider block causing it to tilt. However, the general observed trend shows that k_{setup} is lower than k_{spring}, which is an indication that additional compliant components have a stiffness low enough to influence k_{setup}. The three components that are most likely to influence k_{setup} are the electro motor, load cell and the string connecting the electro motor and spring. Apart from mechanical influences, slow preseismic creep can also lower the slope of the loading curve although this cannot entirely account for the difference between k_{spring} and k_{setup}.

One of the most distinct features of the slip events are the multi-topped velocity curves present during all slip events recorded (fig. 6b). The stepwise displacement occurring during slip has a significant influence on the maximum velocity of the slider block. Through testing it was determined that dilatation of the glass beads layer during slip results in a gravitational effect on the slider block. During a slip event the slider block has to overcome multiple consecutive dilations, which results in a non-uniform displacement and a multi-parabolic velocity curve. The normal force distribution on the slider block enhances this effect. To reduce ploughing, the weights were placed at the back of the slider block. As a result, the normal force is not distributed equally over the surface area of the block, which creates a slight inclination of the slider block with respect to the marble base layer. During a slip event, the glass beads accumulate under the slider block creating a non-uniform surface which the slider block has to overcome. The shear force curve does not show the effects of the stepwise displacement of the slider block during a slip event (fig. 5), which suggests that the effect is too small to be picked up by the load cell or is dampened by the ring connecting the load cell and the slider block. The shear force curve does, however, show a gradual decrease of the slope near the end of the slip event due to the constant loading velocity exerted on the spring.

5.3 Trends observed in the experimental data

The results show dependencies of the displacement dx, force drop dF, maximum velocity Vmax and the recurrence time on the normal load, spring stiffness, load point velocity and the grain size. Comparison between the experimental results and the results from the numerical simulations done by QDYN reveals, in most cases, distinct similarities in both the trends and the absolute values. However, the experimental results vary in quality and are subjected to various experimental artifacts.

The F_n results show a positive linear dependency for all variables measured with good trend fits for dx and Vmax. The dF trend fit is an exception as the experimental values are significantly lower than the QDYN values and are characterized by large standard deviations of up to 28%. In comparison to the other dF results, which have a maximum standard deviation of 10%, this is exceptionally large. As a result k_{setup}, is an order of magnitude lower than k_{spring}. With respect to the other experimental results, the largest difference in the used parameters is the $V_{load\ point}$, which is at least an order of magnitude lower during the other experiments. Both this study and other work (Anthony & Marone, 2005; Wong & Zhao, 1990) show that an increase in $V_{load\ point}$ results in a decrease in stress drop

during stick-slips, which is suspected to be the main explanation for the low dF values. The accompanying large standard deviations are also attributed to the high $V_{load\ point}$. In comparison to the results of QDYN, dF is rather low, but this difference in the absolute values is also observed in the other results.

The k_{spring} experiments show a negative power law dependence of dx, dF, Vmax and the recurrence time on k_{spring}. The resulting trend lines show a good fit for the dx data, while the dF and Vmax results are compromised by an outlier at k_{spring} = 0.8955 N/mm. Ignoring this outlier, results in a good trend fit for both dF and Vmax although the dF values are a factor two lower than the QDYN results. Laboratory experiments performed by Ohnaka (1973), using a servocontrolled biaxial loading apparatus, show a twofold increase in dF when reducing k_{spring} by a factor of 43. Since our results show a negative power law dependency between k_{spring} and dF this relation was not found, but does show an increase in dF when k_{spring} is decreased. Numerical simulations done by Gu and Wong (1991) show comparable results. The trend produced by QDYN confirms the general observations done by Ohnaka (1973) and Gu and Wong (1991) in terms of the magnitude of the effect k_{spring} has on dF. Calculating the k_{setup} from the slope of the load curves reveals a relatively decreasing k_{setup} with an increasing k_{spring}, which has to be taken into account when evaluating the data. Applying this observation to the graph showing the experimental data results in a slightly steeper slope for the experimental results and a greater discrepancy between the experimental data and data produced by QDYN.

When looking solely at the experimental data obtained when varying $V_{load\ point}$ the trend seems to be linear when excluding one outlier at $V_{load\ point}$ = 0.624 mm/s. However, the QDYN results show a logarithmic relation between $V_{load\ point}$ and dx, dF and Vmax that can also fit the experimental data, but is not as apparent. Both rock mechanics and seismological observations agree with the notion that dF decreases with an increasing $V_{load\ point}$. Rock friction experiments performed by several authors e.g. Ohnaka (1973), Englender and Scholz (1976), Teufel and Logan (1978), Shimamoto and Logan (1986), Chester (1988), Lajtai and Gadi (1989) and Wong and Zhao (1990) on halites and silicates using a broad range of configurations and conditions consistently show that dF in stick-slip events decreases with increasing $V_{load\ point}$ (Gu & Wong, 1991). Numerical modeling done by Gu and Wong (1991) confirmed this relation. Anthony and Marone (2005) found that an increase in the loading rate results in a decrease in the stress drop and recurrence time due to the effect of the loading rate on building and breaking of force chains in a granular layer. The logarithmic relationship found between $V_{load\ point}$ and dx, dF and Vmax shows the effect of the healing mechanism on these variables. An increase in the $V_{load\ point}$ decreases the recurrence time and therefore the time μ, which increase according to log t.

The recurrence time is increases with an increasing F_n and decreases with an increasing k_{spring} and grain size. Due to insufficient usable data from the $V_{load\ point}$ experiments, the trend is unknown. However, Anthony and Marone (2005) performed similar experiments, which showed that an increase in $V_{load\ point}$ results in a decrease of the recurrence time. In general, the results show dF increasing with the recurrence time, an observation that is both in line with earlier experimental work and seismological work done on small recurring earthquakes along the Calaveras fault in North California (Nadeau & McEvilly, 1999).

All the experimental data shows an increase in dx and Vmax when increasing dF. This further validates the obtained data, since it is expected a larger dF is accompanied by a larger dx and Vmax.

As expected, the Ottawa sand results are similar to the glass beads results, but due to the sub angular shape of the sand, the slip events are less consistent resulting in significantly higher standard deviations. The observed trends are linear and comparable to the QDYN results. The RSF parameters have been adjusted to fit the experimental data. The most notable difference between the RSF

parameters used for the glass beads and the RSF parameters used for the Ottawa sand experiments is the decrease of D_c, which is attributed to the use of a larger grain size (425-500 µm) and the sub-angular shape of the grains. Due to the use of different parameter values for the glass beads and Ottawa sand experiments, the results are difficult to correlate. The difference in the coefficient of friction observed, is an indication for the effect of the usage of angular grains and a rough friction surface on dx, dF and Vmax. It is expected that these variables are larger when using the Ottawa sand friction volume. Other work using spherical glass beads and Ottawa sand confirms this assumption (Anthony & Marone, 2005; Mair et al., 2002).

A comparison between the glass beads and quartz results is hard to make, since both experiments were done using different parameters. However, angular grains and a rough surface friction have been found to significantly increase µ, Vmax, dF and dx (Anthony & Marone, 2005) and these relations are also expected for results obtained by our experimental setup.

QDYN's spring slider model has proven to be a useful analog for its experimental equivalent using glass beads as the fault gouge. However, since the models quasi-dynamic inertial effects are only accounted for through a radiation damping term, QDYN cannot be considered a one on one analog with nature. Thomas et al. (2014) compared quasi-dynamic versus fully dynamic simulations in a 2D setting using standard RSF friction and relatively uniform fault properties. The results where qualitatively similar in terms of earthquake patterns and crack-like ruptures, but the quantitative differences where significant with larger amounts of slip per event, larger stress drops and significantly higher velocities and rupture speeds (Thomas et al., 2014). Although these results are calculated using a 2D surface it is expected that the same relation can be applied when simulating a spring slider system. Using large-scale simulation models, such as QDYN, to simulate the size of an earthquake is possible, but the limitation of a quasi-dynamic model should always be taken into consideration. The same concept can be applied to the results in this study, but due to the scale of the experimental results obtained in this study, the difference between model and experimental results is significantly smaller. When taking into account the computation and time costs of using a fully dynamic model, using such a model is not worthwhile when simulating a spring slider experiment.

5.4 Trends not observed in the experimental data

The grain size experiments show a large scatter in the data with no consist trends that might not be related to the results produced by QDYN. The k_{setup} reveals a similar pattern with grain sizes 160-210 µm and 400-500 µm results that lie close to the actual k_{spring} and grain sizes 300-400 µm and 400-500 µm that have a low k_{setup}. Overall, no trends can be observed from the grain size data. Because the grain size is not a parameter in QDYN, D_c was taken as an equivalent for the grain size. D_c and grain size should be related with one another, since the characteristic slip distance required to renew the surface contacts is depending on the amount of grains per surface area that influence the surface contacts. While this relation is most definitely present, interaction between grains also has a significant effect on the macroscopic friction of the granular volume. The applied shear force on a granular layer is accommodated by force chains of various geometries that affects the frictional stability (Mair et al., 2002). Because of the way the experiment is set up grains also accumulate in between the side of the slider block and the sidewalls, which creates an additional friction surface and although no direct force is applied on this surface different grain sizes can affect the friction on this surface. The trends produced by QDYN may therefore not be partly representative for the effect of grain size on the experimental results. In contrast to the results of this study Anthony and Marone (2005) were able to determine a relation between grain size and dF and found that an increase in the grain size results in an increase in the stress drop. This is inconsistent with the results produced by QDYN, which shows a negative linear dependence of dF with D_c. These observations indicate that D_c

cannot be directly used as a substitute for grain size in QDYN. It has to be noted that the experiments of Anthony and Marone (2005) were done at higher stress levels (σ_n = 10 MPa) and with a double direct shear configuration, but this is not expected to have a result on the slope of dF with grain size.

Since QDYN has proven to be a useful analog for a spring slider system the effect of (a-b) and D_c have been investigated using QDYN. The trends observed for dx, dF and Vmax when varying F_n are linear. (a-b) has an amplifying effect on the slope of the variables. Since this data is derived from simulations done at a low F_n translating this data to natural conditions would mean a large effect of (a-b) on the magnitude of an earthquake. D_c does not seem to have a large effect on the slope of dx, dF and Vmax. However, it seems that when D_c decreases the slope increases slightly for both the dF and Vmax data. It has to be noted that both variables are represented by QDYN in three decimals, therefore the data is subjected to a certain margin of error that could influence the slope. While both dx and dF increase when D_c increases, Vmax decreases.

5.5 Comparison with trends observed in nature

The trends observed in the experimental data and in the results from QDYN are based on a system where only one variable is changed whilst the others are kept constant. This approach ensures isolated data on the effects of these variables and enables comparison between trends observed in the laboratory and those obtained from models. Although a comparison can be made between laboratory results and natural events, they latter are influenced by external factors such as the heterogeneity and complexity of existing fault systems, the stress conditions at large depth, influence of existing faults, hydrothermal conditions and the chemical processes occurring in faults. Additionally, recreation of natural events is difficult considering the complexity in distribution of the RSF parameters.

Induced seismicity events are less affected by such external factors because of their smaller size and might be a better analog of laboratory experiments while still occurring in a heterogeneous natural environment. Warpinsky and Zimmer (2012) observed thousands of induced seismicity events associated with hydraulic fracturing in six major shale basins in North America and found an increase of magnitude with depth (1-4 km), which is in accordance with laboratory results when relating an increase in normal stress with an increase in depth. The difference between the shallow and deep micro seismic magnitudes was found to be up to 2.5 to 3 magnitude units depending on the shale basin again indicating that depth is not the only parameter affecting the magnitude of an earthquake. At larger depths the same observations were made and it was found that a large volume change results in larger magnitudes, larger stress disturbance and a higher chance of reactivating an existing fault structure (Buijze, 2015). In nature, the largest events occur when large fault structures are reactivated, which is not necessarily linked to depth and adds another layer of complexity. Evans et al. (2012) found that hydraulic fracturing in sedimentary rock is less seismogenic than in crystalline rocks identifying the importance of rock composition and thus frictional properties on the nature of seismicity. Another observation made with regards to induced seismicity is the low stress drop associated with induced events in comparison to natural events (Buijze, 2015). Nevertheless, it is perhaps possible to use data gained from induced seismicity events to extract RSF parameters using a numerical model such as QDYN. Since this study only used the spring slider analog of QDYN and the acquired data is therefore not suited to be directly applied to a more complex situation, an effort has to be made to determine the effect of the RSF parameters using a 3D model.

6. Conclusion

Spring slider experiments were performed with a varying normal load, spring stiffness, load point velocity and grain size to determine the influence of these parameters on the displacement, force drop, maximum velocity and the reoccurrence time of a slip event and to validate the numerical

model QDYN. We found that QDYN provides to be a useful analog for a spring slider system. In addition, we used the experimental results to validate the results of a numerical model, called QDYN. In general, we found that the numerical results produced by QDYN compare favorably with the experimental results obtained using a spring slider system. The effect of quartz sand on the size (i.e. the displacement, force drop and maximum velocity) of a slip event were investigated. The effect of (a-b) and D_c on the size of unstable stick-slip events ('earthquakes'), while also varying the normal load, was investigated.

The results are summarized as follows:
- Experimentally we found convincing trends of the amount of displacement as a function of the used parameters (i.e. normal load, spring stiffness and load point velocity). These trends are respectively linear, power law and logarithmic trends and the slopes are similar to those obtained using the numerical model.
- Convincing trends were also found of the amount of force drop as a function of the used parameters. These trends are respectively linear, power law and logarithmic trends and the slopes are similar to those obtained using the numerical model.
- We found convincing trends of the amount of maximum velocity as a function of the used parameters. These trends are respectively linear, power law and logarithmic trends and the slopes are similar to those obtained using the numerical model.
- The recurrence time as a function of the normal load, spring stiffness and grain size shows linear, power law and linear trends respectively.
- The other parameters do not show convincing trends, even though the numerical model suggests there is a trend.
- The effect of varying grain size, as an equivalent of fault gouge, on the used parameters shows no clear trends. D_c was taken as an equivalent for the grain size to enable a comparison between the spring slider and QDYN. We found that in our setup, D_c could not be used the equivalent of grain size, because of other effects of the grain size on macroscopic friction. It might be possible to mitigate these effects (perhaps by using a single layer of beads) and directly link grain size to D_c.

- The experiments done using angular sand as the friction volume, show similar results to the experiments done with glass beads. Although the results are difficult to correlate due to the use of different experiment parameters the coefficient of friction is higher when using angular sand (μ = 0.356) instead of glass beads (μ = 0.278), which is expected because of the use of a sandstone block with a rough surface friction and because of the use of angular grains. The size of a slip event is expected to increase under these conditions.
- All of the experiments show a linear increase in the total amount of displacement and the maximum slip velocity when the concomitant force drop increases.
- Non-uniform dilatation along the gouge layer during the slip event results in multiple acceleration and deceleration phases, effectively lowering the maximum slip velocity.
- Fitting rate-and-state parameters to experimental data, obtained from stick-slip experiments using glass beads as a friction volume, has proved to be applicable when these parameters cannot be determined through velocity stepping experiments.
- To investigate the effect of RSF parameters on the relation between the normal load and the size of an event, multiple simulation with varying RSF parameters were performed. An increase in (a-b) results in an increase in both the slope and the absolute values of the displacement, force drop and maximum velocity. An increase in D_c has no significant effect on the slope of the displacement, force drop and maximum velocity. D_c increases the absolute values of the displacement and force drop,

but decreases the maximum velocity. Since D_c is related to the real contact area this observation shows that an increase in the real contact area results in an increase in the displacement and force drop and in a decrease of the maximum velocity.
- It is perhaps possible to use QDYN to extract rate-and-state friction parameters from seismological data of natural events. Since natural events are influenced by a large number of factors they are hard to simulate in a laboratory environment. Induced seismicity events are better suited to provide quantitative and consistent data to extract rate-and-state friction data from.
- When the RSF parameters are known, large-scale simulation models, such QDYN, can be used to approximate the size of an earthquake, however on such a large scale additional factors, such as the inertial effects, have a significant effect. The limitations of quasi-dynamic numerical models should, therefore, always be taken into consideration when simulating natural events.

References

Amontons, G. (1699), Method of substituting the force of fire for horse and man power to move machines. Histoire et Mémoires de l'Académie Royale des Sciences, pp.112.

Anthony, J.L. & C. Marone. (2005), Influence of particle characteristics on granular friction. Journal of Geophysical Research: Solid Earth (1978–2012) 110(B8)

Bowden, F.P. & D. Tabor. (1950), The Friction and Lubrication of Solids (Part I).

Bowden, F.P. & D. Tabor. (1964), The friction and lubrication of solids (Part 2).

Brace, W.F. (1972), Laboratory studies of stick-slip and their application to earthquakes. Tectonophysics 14(3–4), pp.189-200.

Brace, W.F. & J.D. Byerlee. (1966), Stick-slip as a mechanism for earthquakes. Science 153(3739), pp.990-992.

Buijze, A.J.L. (Unpublished),

Byerlee, J. (1978), Friction of rocks. Pure and Applied Geophysics PAGEOPH 116(4-5), pp.615-626.

Byerlee, J.D. (1970), The mechanics of stick-slip. Tectonophysics 9(5), pp.475-486.

Carlson, J. & J. Langer. (1989), Mechanical model of an earthquake fault. Physical Review A 40(11), pp.6470.

Chester, F.M. (1988), The brittle-ductile transition in a deformation-mechanism map for halite. Tectonophysics 154(1), pp.125-136.

Dieterich, J.H. (1986), A model for the nucleation of earthquake slip. Earthquake source mechanics, pp.37-47.

Dieterich, J.H. (1979), Modeling of rock friction 1. Experimental results and constitutive equations. Journal of Geophysical Research: Solid Earth 84(B5), pp.2161-2168.

Engelder, J. & C.H. Scholz. (1976). The role of asperity indentation and ploughing in rock friction—II: Influence of relative hardness and normal load. Paper presented at the International Journal of Rock Mechanics and Mining Sciences & Geomechanics Abstracts, , 13(5) pp.155-163.

Evans, K.F., A. Zappone, T. Kraft et al. (2012), A survey of the induced seismic responses to fluid injection in geothermal and CO2 reservoirs in Europe. Geothermics 41(0), pp.30-54.

Freedman, D. & P. Diaconis. (1981), On the histogram as a density estimator:L2 theory. Zeitschrift für Wahrscheinlichkeitstheorie und Verwandte Gebiete 57(4), pp.453-476.

Gu, Y. & T. Wong. (1991), Effects of loading velocity, stiffness, and inertia on the dynamics of a single degree of freedom spring-slider system. Journal of Geophysical Research: Solid Earth (1978–2012) 96(B13), pp.21677-21691.

He, C., T. Wong & N.M. Beeler. (2003), Scaling of stress drop with recurrence interval and loading velocity for laboratory-derived fault strength relations. Journal of Geophysical Research: Solid Earth 108(B1), pp.n/a-n/a.

Hori, T., N. Kato, K. Hirahara et al. (2004), A numerical simulation of earthquake cycles along the Nankai Trough in southwest Japan: lateral variation in frictional property due to the slab geometry controls the nucleation position. Earth and Planetary Science Letters 228(3), pp.215-226.

Karner, S.L. & C. Marone. (2000; 2013). Effects of loading rate and normal stress on stress drop and stick-slip recurrence interval. Geocomplexity and the Physics of Earthquakespp. 187-198American Geophysical Union.

Lajtai, E. & A. Gadi. (1989), Friction on a granite to granite interface. Rock Mechanics and Rock Engineering 22(1), pp.25-49.

Lapusta, N. (2000), Elastodynamic analysis for slow tectonic loading with spontaneous rupture episodes on faults with rate- and state-dependent friction. Journal of Geophysical Research: Solid Earth 105(B10), pp.23765-23789.

Lapusta, N., J.R. Rice, Y. Ben-Zion et al. (2000), Elastodynamic analysis for slow tectonic loading with spontaneous rupture episodes on faults with rate- and state-dependent friction. Journal of Geophysical Research: Solid Earth 105(B10), pp.23765-23789.

Louis, L., C. David & P. Robion. (2003), Comparison of the anisotropic behaviour of undeformed sandstones under dry and saturated conditions. Tectonophysics 370(1–4), pp.193-212.

Mair, K., K.M. Frye & C. Marone. (2002), Influence of grain characteristics on the friction of granular shear zones. Journal of Geophysical Research: Solid Earth 107(B10), pp.ECV 4-1-ECV 4-9.

Mair, K. & C. Marone. (1999), Friction of simulated fault gouge for a wide range of velocities and normal stresses. Journal of Geophysical Research: Solid Earth 104(B12), pp.28899-28914.

Marone, C. (1998). Laboratory-derived friction laws and their application to seismic faulting Retrieved 9 January 2015.

Marone, C., B. Carpenter & P. Schiffer. (2008), Transition from rolling to jamming in thin granular layers. Physical Review Letters 101(24), pp.248001.

Nadeau, R.M., A. Michelini, R.A. Uhrhammer et al. (2004), Detailed kinematics, structure and recurrence of micro-seismicity in the SAFOD target region. Geophysical Research Letters 31(12)

Nadeau, R.M. & T.V. McEvilly. (1999), Fault Slip Rates at Depth from Recurrence Intervals of Repeating Microearthquakes. Science 285(5428), pp.718-721.

Nasuno, S., A. Kudrolli & J.P. Gollub. (1997), Friction in granular layers: Hysteresis and precursors. Physical Review Letters 79(5), pp.949-952.

Niemeijer, A., G. Di Toro, W.A. Griffith et al. (2012), Inferring earthquake physics and chemistry using an integrated field and laboratory approach. Journal of Structural Geology 39(0), pp.2-36.

Ohnaka, M. (1973), Experimental studies of stick-slip and their application to the earthquake source mechanism. Journal of Physics of the Earth 21(3), pp.285-303.

Rabinowicz, E. (1956), Stick and slip. Scientific American 194, pp.109-119.

Rabinowicz, E. (1951), The Nature of the Static and Kinetic Coefficients of Friction. Journal of Applied Physics 22(11), pp.1373-1379.

Rabinowicz, E. (1958), The intrinsic variables affecting the stick-slip process. Proc.Phys.Soc. 71, pp.668-675.

Rice, J.R. & S.T. Tse. (1986), Dynamic motion of a single degree of freedom system following a rate and state dependent friction law. Journal of Geophysical Research 91(B1), pp.521-530.

Ruina, A. (1983), Slip instability and state variable friction laws. Journal of Geophysical Research 88(B12), pp.10359-10370.

Rundle, J.B. & D.D. Jackson. (1977), Numerical simulation of earthquake sequences. Bulletin of the Seismological Society of America 67(5), pp.1363-1377.

Scholz, C. H. (2002). The mechanics of earthquakes and faultingCambridge university press.

Scholz, C.H., P. Molnar & T. Johnson. (1972), Detailed studies of frictional sliding of granite and implications for the earthquake mechanism. Journal of geophysical research 77(32), pp.6392-6406.

Scholz, C. H.,. (1990). The mechanics of earthquakes and faulting. New York: Cambridge University Press.

Shimamoto, T. & J.M. Logan. (1986), Velocity-Dependent Behavior of Simulated Halite Shear Zones: An Analog for Silicates. Earthquake source mechanics, pp.49-63.

Teufel, L. & J. Logan. (1978), Effect of displacement rate on the real area of contact and temperatures generated during frictional sliding of Tennessee sandstone. Pure and Applied Geophysics 116(4-5), pp.840-865.

Thomas, M.Y., N. Lapusta, H. Noda et al. (2014), Quasi-dynamic versus fully dynamic simulations of earthquakes and aseismic slip with and without enhanced coseismic weakening. Journal of Geophysical Research: Solid Earth 119(3), pp.1986-2004.

Wong, T. & Y. Zhao. (1990), Effects of load point velocity on frictional instability behavior. Tectonophysics 175(1–3), pp.177-195.

Acknowledgements

First and foremost, I would like to express my gratitude towards my supervisor Dr. André Niemeijer, who has provided me with excellent guidance and feedback. Without it I would have been lost. I want to express my gratitude towards Evangelos Korkolis and Martijn van den Ende as well for listening to my problems, providing feedback and coming up with great solutions. My thanks go to Loes Buijze as well for giving me a great introduction into QDYN and numerical modelling in general. Furthermore I would like to thank the technicians the HPT lab in Utrecht for providing and building the equipment I needed. A thanks goes out to Dr. Suzanne Hangx who provided my with the Ottawa sand. I thank Prof. Dr. Chris Spiers for being my second supervisor. Last but not least, I want to thank all the people at the HPT lab for their interest, help and good times.

Appendix A

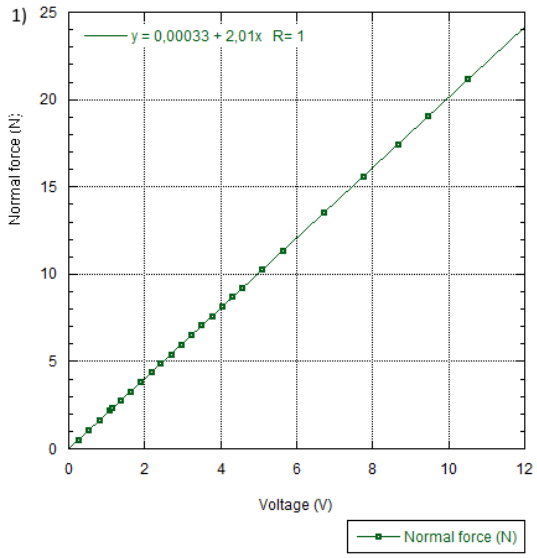

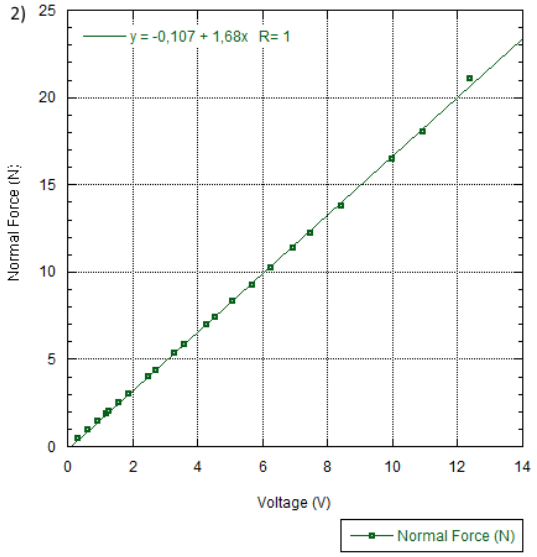

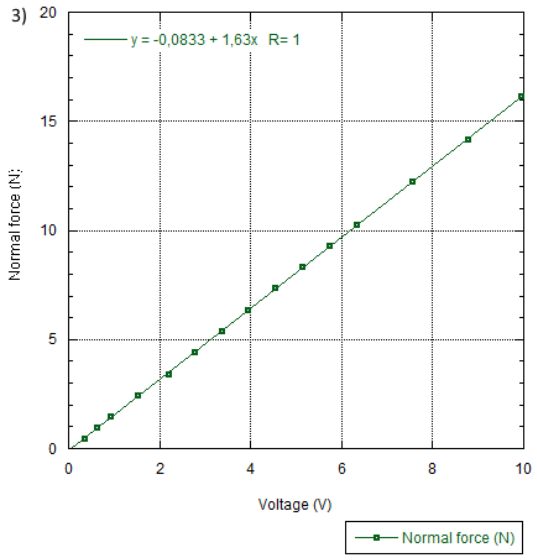

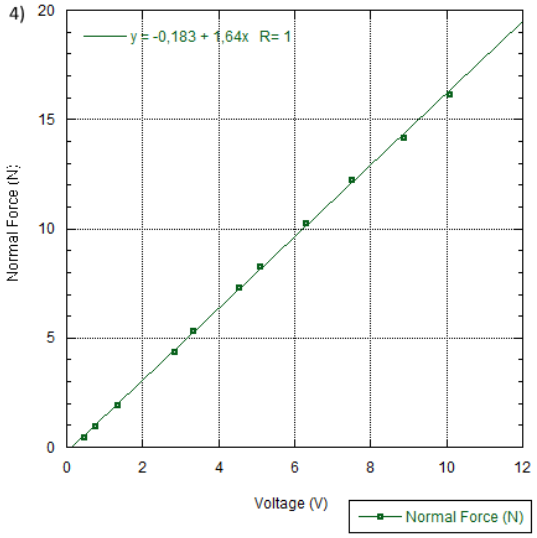

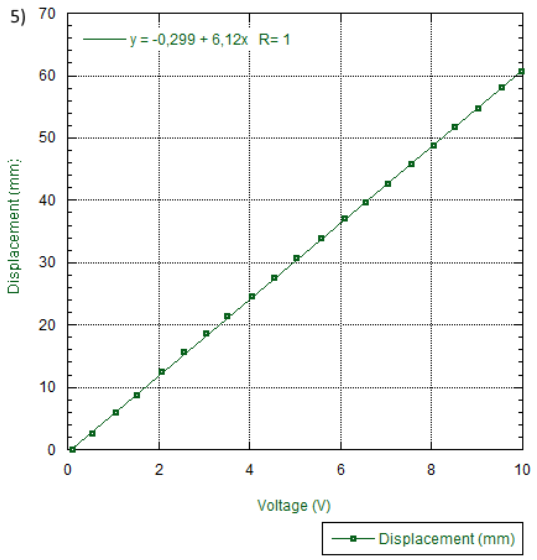

Overview of the calibration curves of the load cell (1, 2, 3, 4) and the potentiometer (5). The calibration curves of the load cell are shown in chronological order.

Appendix B

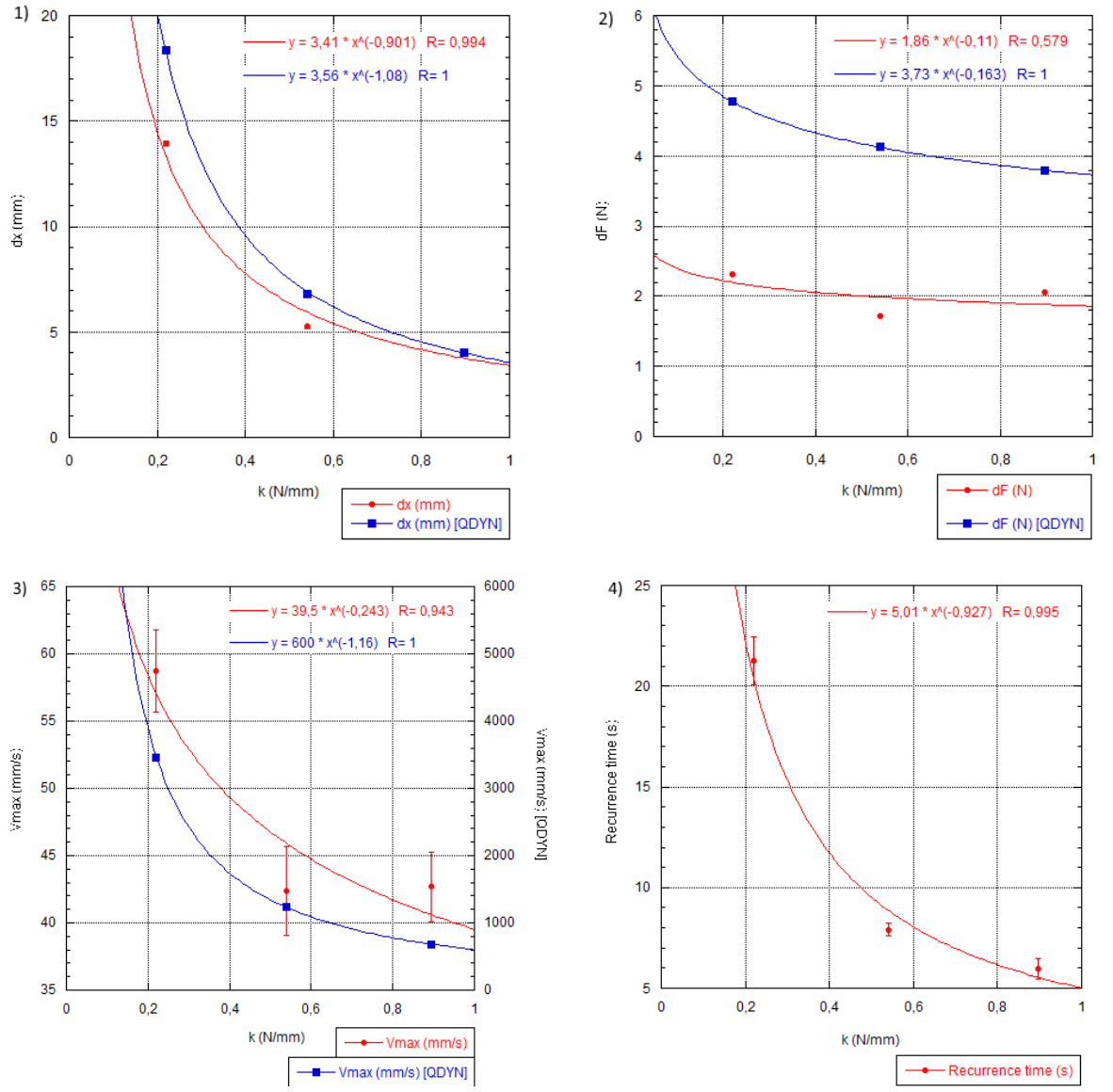

Overview of experimental and QDYN data showing the effect of the spring stiffness on the displacement, force drop, maximum velocity and recurrence time. The following parameters where used: F_n = 36.12 N, $V_{load\ point}$ = 0.624 mm/s and grain size = 150-210 µm.

Appendix C

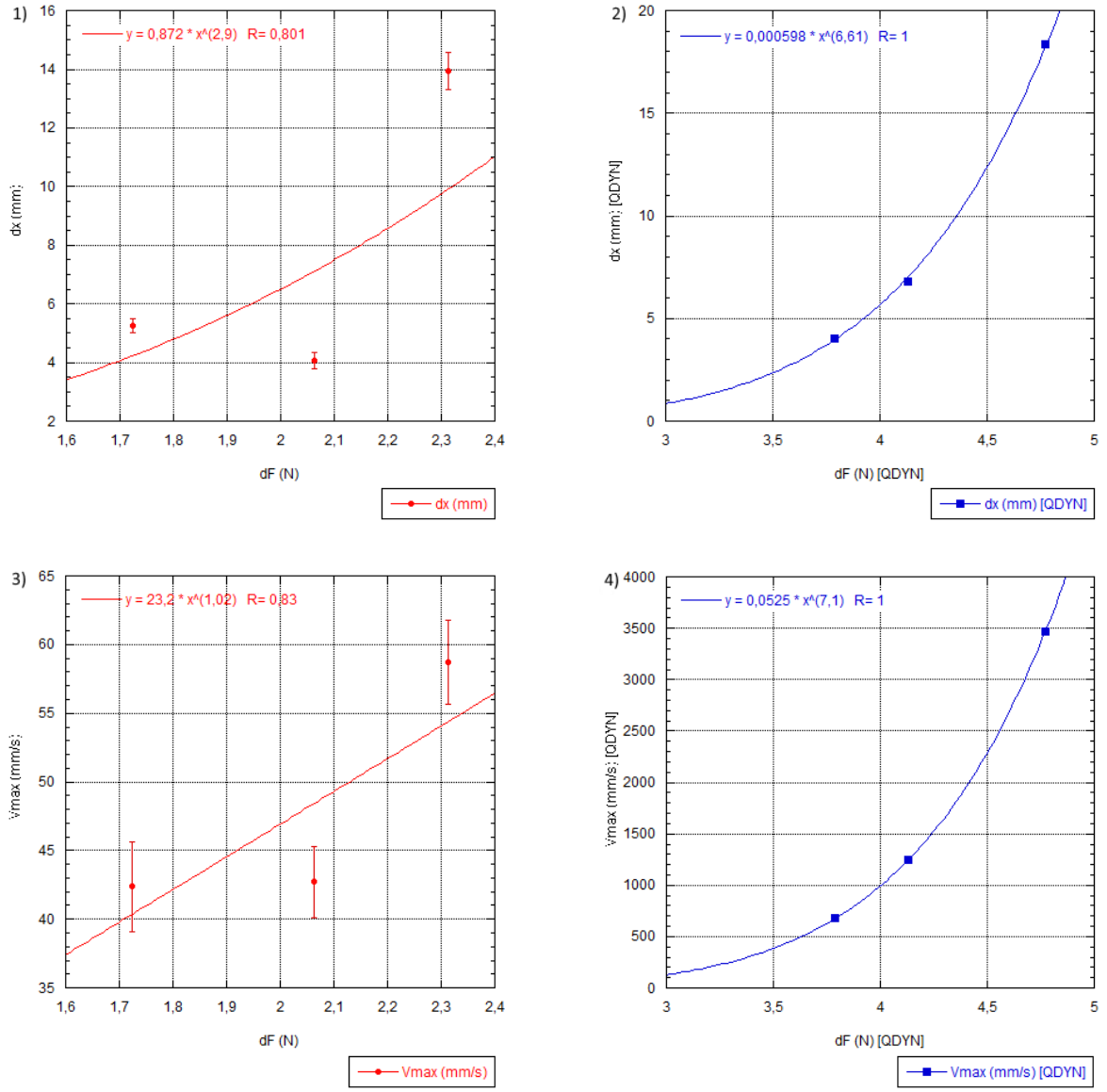

Overview of experimental and QDYN data showing how the displacement and maximum velocity are effected by the force drop, while varying the spring stiffness. The following parameters where used: F_n = 36.12 N, $V_{load\ point}$ = 0.624 mm/s and grain size = 150-210 µm.

Appendix D

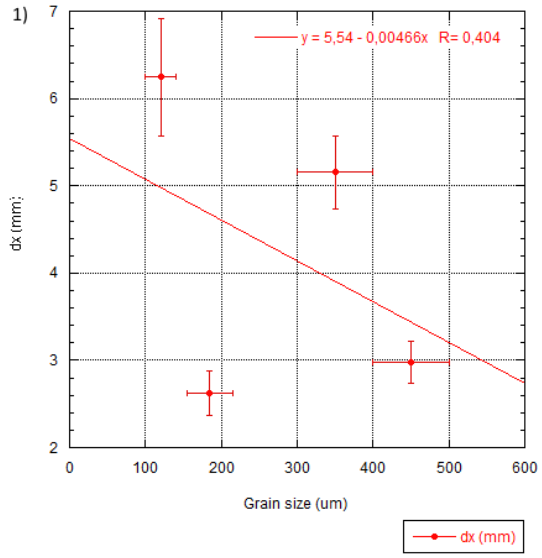

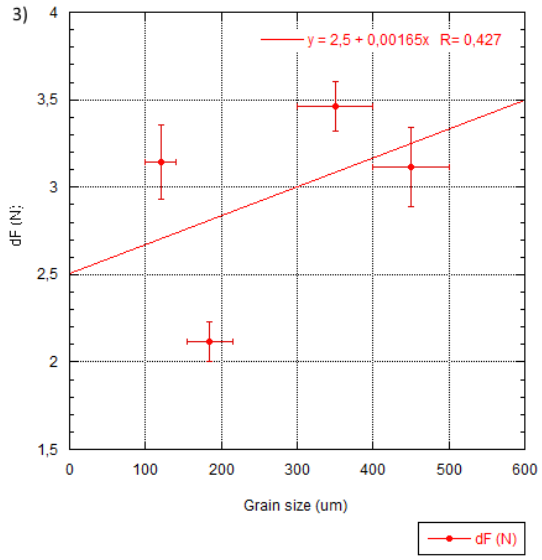

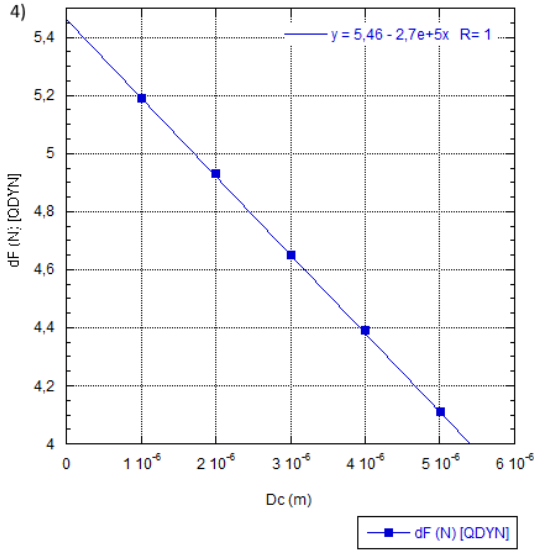

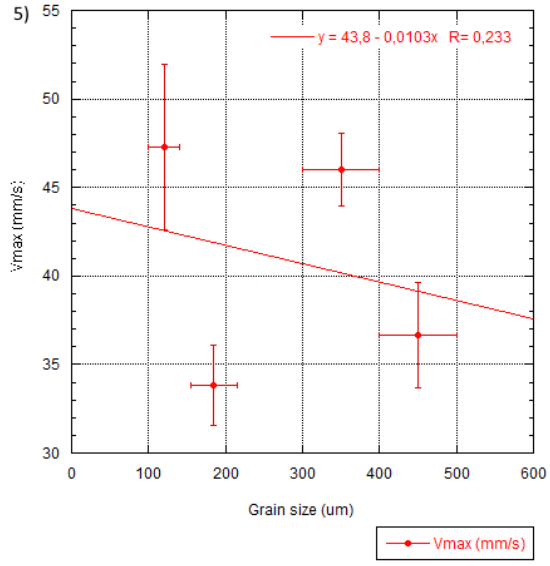

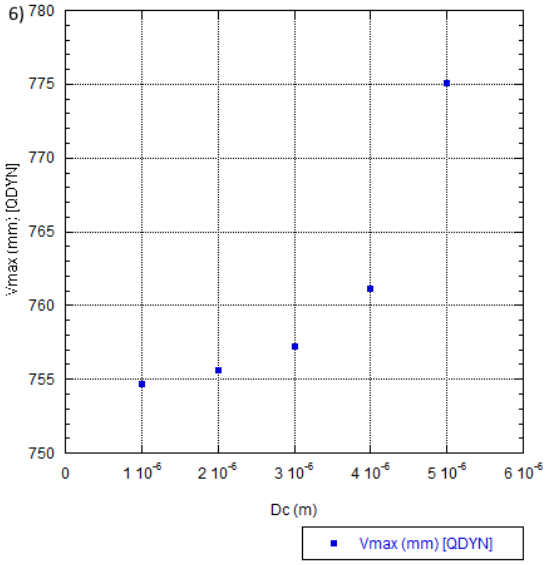

Overview of experimental and QDYN data showing the effect of the grain size on the displacement, force drop, maximum velocity. The following parameters where used: F_n = 36.12 N, k = 0.8955 N/mm and $V_{load\ point}$ = 0.1248 mm/s.

Appendix E

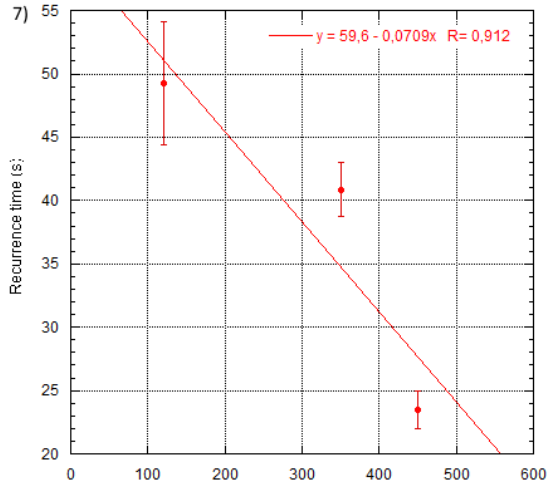

Overview of experimental and QDYN data showing the effect of the grain size on the recurrence time. The following parameters where used: F_n = 36.12 N, k = 0.8955 N/mm and $V_{load\ point}$ = 0.1248 mm/s.

Appendix F

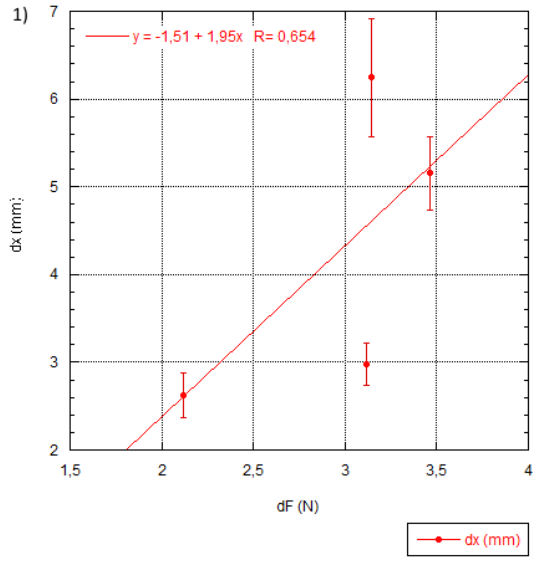

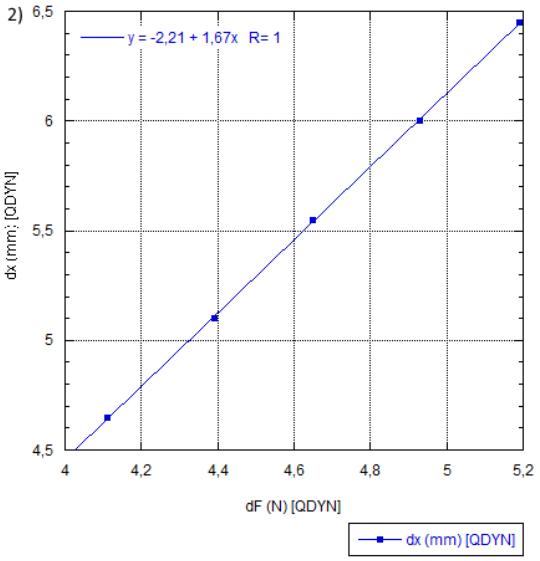

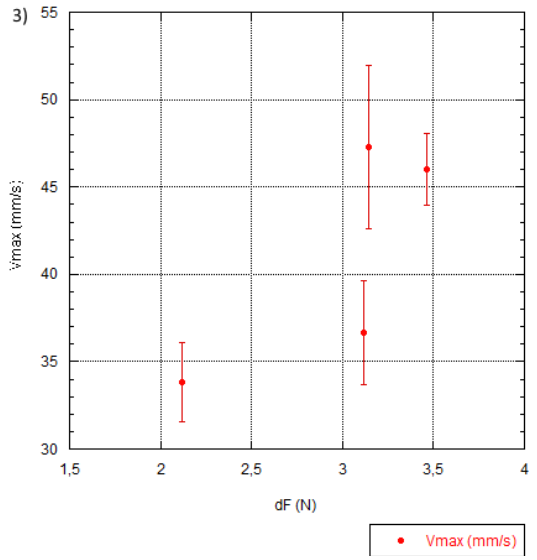

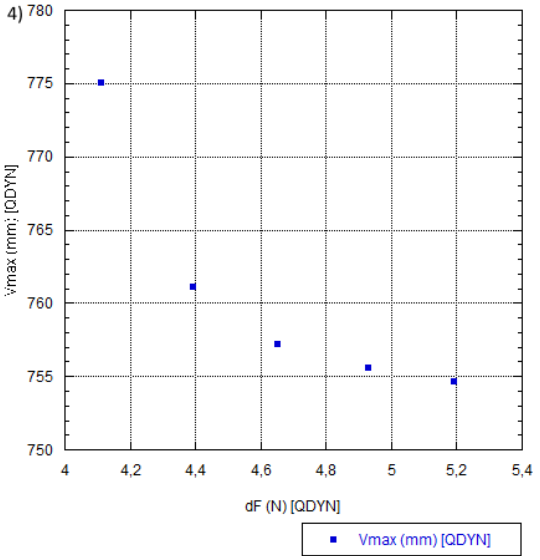

Overview of experimental and QDYN data showing how the displacement and maximum velocity are effected by the force drop, while varying the grain size. The following parameters where used: F_n = 36.12 N, k = 0.8955 N/mm and $V_{load\ point}$ = 0.1248 mm/s.

Appendix G

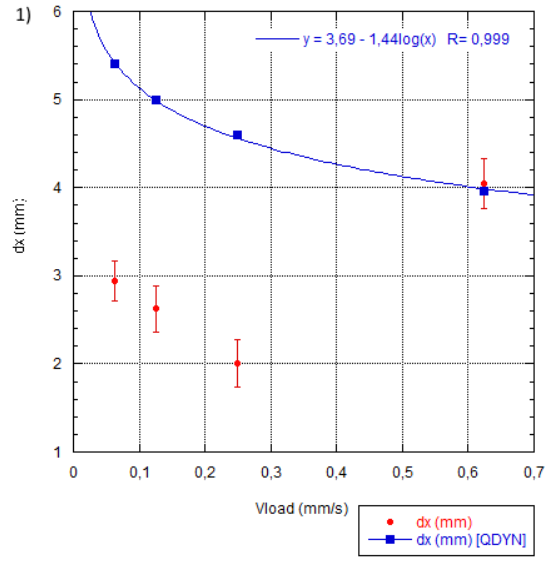

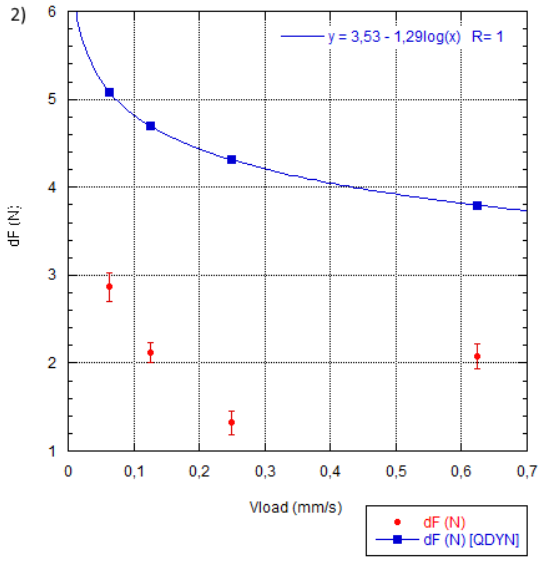

Overview of experimental and QDYN data showing the effect of the load point velocity on the displacement, force drop, maximum velocity. The recurrence time plot is not shown, due to insufficient data. The following parameters where used: F_n = 36.12 N, k = 0.8955 N/mm and grain size = 150-210 µm.

Appendix H

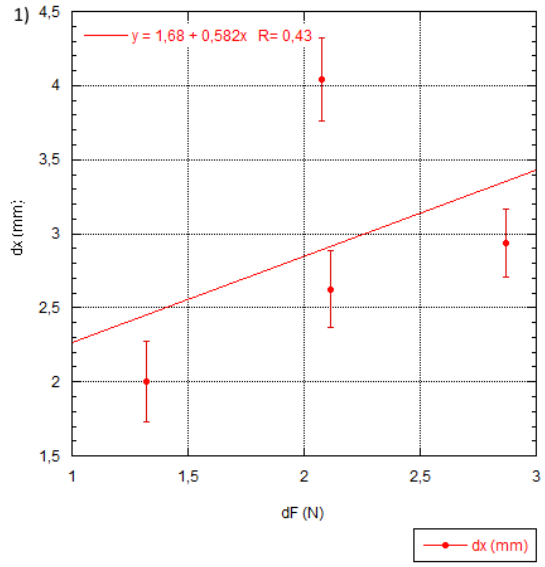

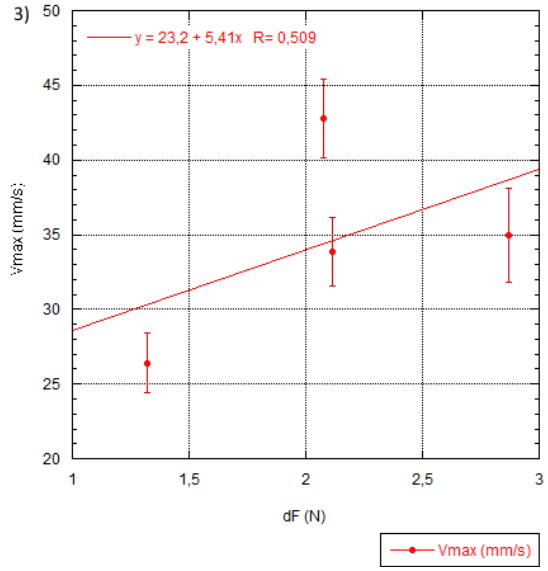

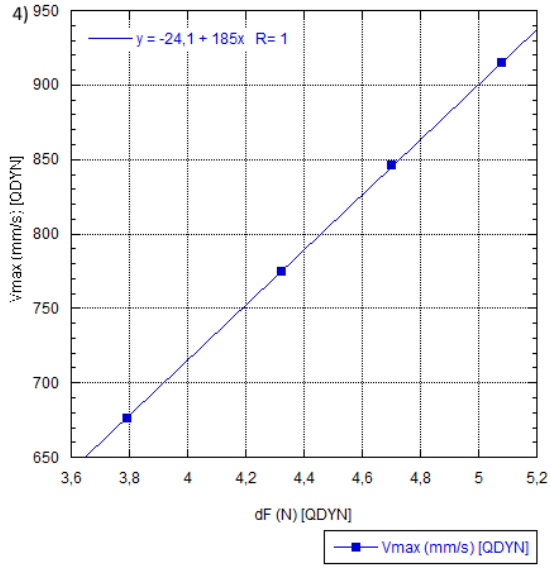

Overview of experimental and QDYN data showing how the displacement and maximum velocity are effected by the force drop, while varying the load point velocity. The following parameters where used: F_n = 36.12 N, k = 0.8955 N/mm and grain size = 150-210 µm.

Appendix J

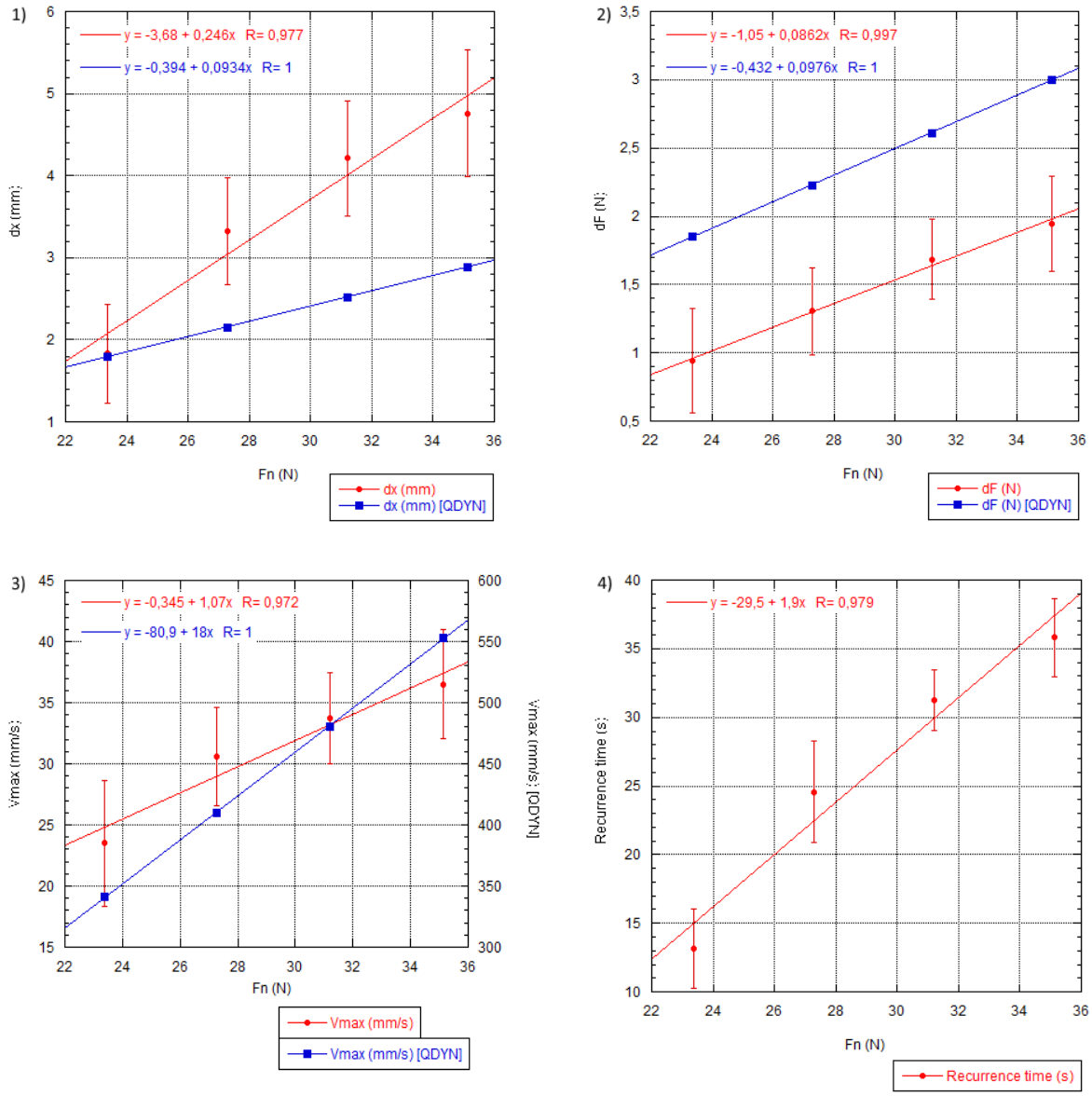

Overview of experimental and QDYN data showing the effect of the normal load on the displacement, force drop, maximum velocity and recurrence time. Quartz sand was used as the friction volume. The reoccurrence time plot is not shown, due to insufficient data. The following parameters where used: F_n = 36.12 N, $V_{load\ point}$ = 0.624 mm/s and grain size = 425-500 µm.

Appendix K

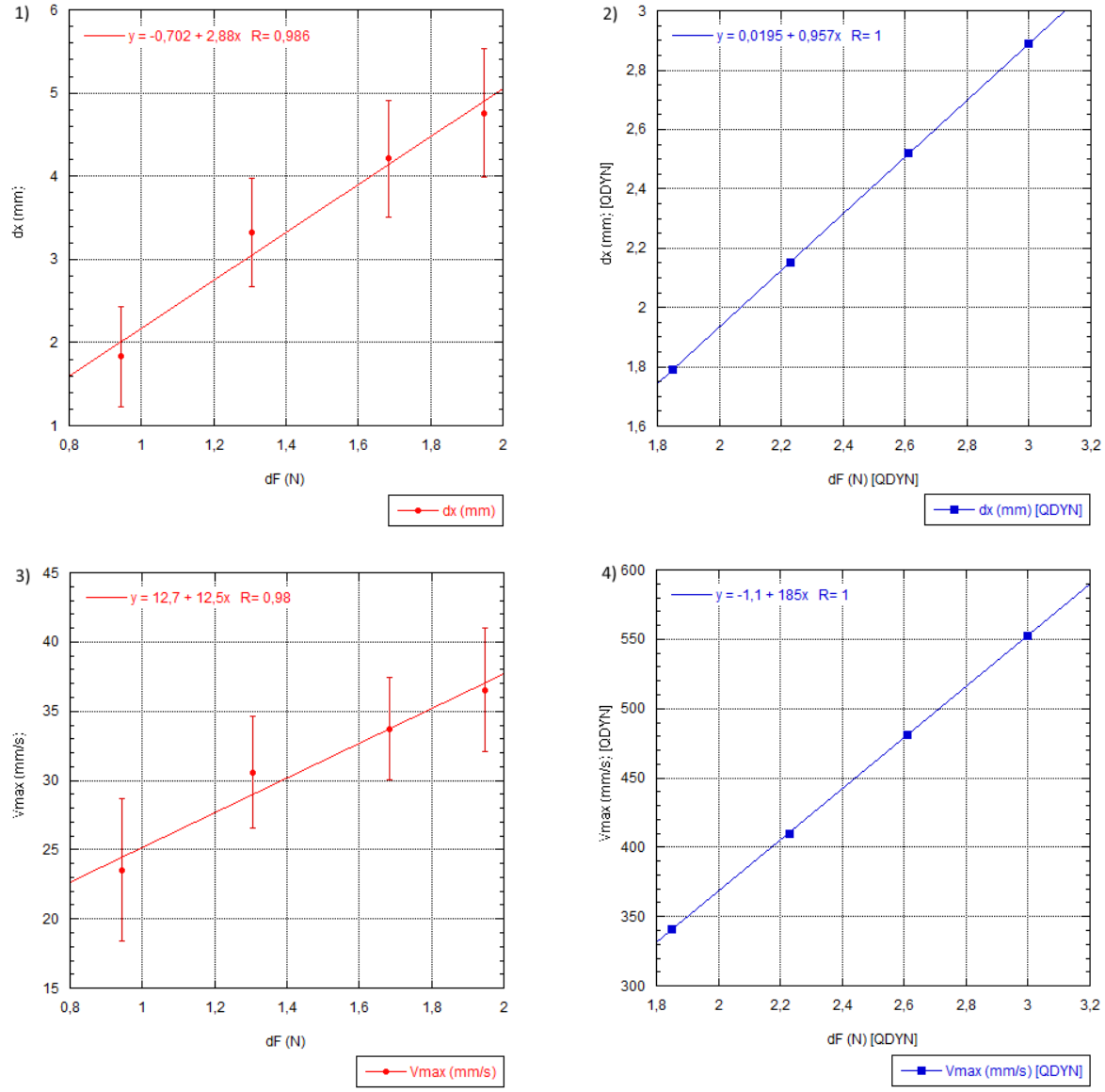

Overview of experimental and QDYN data showing how the displacement and maximum velocity are effected by the force drop, while varying the normal load. Quartz sand was used as the friction volume. The friction volume consists of quartz sand. The following parameters where used: k = 0.8955 N/mm, $V_{load\ point}$ = 0.1248 mm/s and grain size = 4250-500 µm.